To the Graduate Council:

I am submitting herewith a thesis written by Nefi Negrete entitled "Finite Element Investigation of Steady & Unsteady Quasi One-Dimensional Gas Dynamic Flows with Wall Friction and Heat Transfer." I have examined the final paper copy of this thesis for form and content and recommend that it be accepted in partial fulfillment of the requirements for the degree of Master of Science, with a major in Mechanical Engineering.

Dr. Joe Iannelli, Major Professor

We have read this thesis and recommend its acceptance:

Acceptance for the Council:
Vice Provost and Dean of
Graduate Studies

Thesis
2002
.N447

Finite Element Investigation of Steady and Unsteady Quasi One-Dimensional Gas Dynamic Flows with Wall Friction and Heat Transfer

A thesis
Presented for the
Master of Science
Degree
The University of Tennessee, Knoxville

Nefi Negrete

August 2002

DEDICATION

This thesis is dedicated to the three most important women in my life: my loving wife Bridget Negrete, my mother Anna Regagnon, and my late grandmother Ana Acevedo.

ACKNOWLEDGMENTS

I would like to thank Dr. Iannelli for his guidance, support and encouragement throughout my academic life at the University of Tennessee. Without Dr. Iannelli's help, this project would not have been possible. I would like to thank Dr. Wang and Dr. Milligan for serving on the thesis committee.

I would also like to thank my mother for her support and encouragement she has unselfishly given me. Last, but most definitely not least, I would like to acknowledge my boundless gratitude to my lovely wife for her patience and support on the dawn of our new life together.

ABSTRACT

This study developed and validated a finite element procedure to investigate both steady and unsteady gas dynamic flows. Variable cross-sectional area, wall friction, and heat transfer within the duct affect compressible flows. Closed form solutions exist for steady flows determined by only one of these effects at a time. A quasi one dimensional algorithm was refined to combine all of these effects into multiple simulations. Moreover, the effects of an unsteady back pressure were also investigated and compared to the steady results. The back pressure was varied sinusoidally.

The convergent divergent nozzle used had an outlet to throat ratio of 1.5 and a friction coefficient $f = 0.005$ (or $f = 0.02$) depending on how the coefficient is defined. The steady results indicated that for this type of nozzle, friction effects could be neglected while the effects of heat transfer significantly affected the flow. For specific magnitudes of heating, the normal shock found in the diverging nozzle disappeared and the flow became subsonic throughout the nozzle.

An important question was how the flow reacts to a periodic unsteady back pressure. The exit speed, density, and temperature had the same fundamental frequency than the pressure although the unsteady flow was positioned behind the steady due to inertia.

TABLE OF CONTENTS

LIST OF FIGURES

NOMENCLATURE

A	Cross-sectional Area
A_w	Wetted Area
A^*	Reference Area
a	Speed of Sound
c_p	Constant Pressure Specific Heat
c_v	Constant Volume Specific Heat
D	Diameter
D_H	Hydraulic Diameter
E	Total Energy
f	Friction coefficient
M	Mach Number
m	Linear Momentum
$\dot{m}$	Mass Flow Rate
P	Pressure
p_{ref}	Reference Pressure
p_o	Stagnation Pressure
p_t	Stagnation (Total) Pressure
p^*	Reference Pressure
$\dot{q}$	Heat Transfer Rate
R	Gas Constant
T	Temperature
T_{ref}	Reference Temperature
T_o	Stagnation Temperature
T_t	Stagnation (Total) Temperature
T^*	Reference Temperature (flows with friction or heat transfer)
u	Velocity
V	Velocity

Greek

γ	Gas Specific Heat Ratio
ρ	Density
ρ_{ref}	Reference Density
ρ_o	Stagnation Density

1. Objective

This study develops and validates a finite element procedure to investigate both steady and unsteady flows. The specific accomplishments of this investigation are:

1. Derived and added to gas dynamic adiabatic-flow equations specific terms that model wall friction and heat transfer effects.
2. Refined computational procedure to calculate shockless & shocked steady and unsteady flows with simultaneous variable cross-sectional area, wall friction, and heat transfer.
3. Investigated shockless and shocked steady flows as a function of
    a. Cross-sectional variable cross-sectional area.
    b. Wall friction.
    c. Heat transfer.
    d. Wall friction & heat transfer.
    e. Wall friction & variable cross-sectional area.
    f. Heat transfer & variable cross-sectional area.
    g. Wall friction, heat transfer, variable cross-sectional area.
4. Investigated shockless and shocked unsteady flows with
    a. Variable cross-sectional area.

b. Wall friction.

c. Wall friction & variable cross-sectional area.

d. Heat transfer & variable cross-sectional area.

e. Wall friction, heat transfer, variable cross-sectional area.

2. Introduction

Several effects determine compressible flows. Among them are variable cross-sectional area changes, friction, and heat transfer within the duct. The specific geometry of the duct, upstream total energy and density, and downstream pressure determine a compressible flow within a duct. Closed-form solutions exist only for steady flows as a function of only one of these effects acting separately. Either the problem focuses mainly on one of these effects, or including more than one at a time makes the problem intractable for an analytical solution. Furthermore, most solutions correspond to steady flows because many operating situations correspond to a constant back pressure. This project develops and validates a finite element procedure to investigate both steady and unsteady gas dynamic flows determined under the simultaneous effect of area changes, friction, and heat transfer:

A quasi one dimensional finite element code used for investigating adiabatic gas dynamics flows was written by Dr. Iannelli in the programming language C [1]. It requires the initial boundary conditions and the back pressure in order to solve for the flow conditions. The boundary conditions required reflect most real world problems where the back pressure is known and it is desired to predict the flow conditions throughout the flow duct. The results obtained reflect the analytical solutions found in literature. Correct calculations of flows with shock have been obtained.

This project has refined the code to combine all of these effects into multiple simulations. These simulations simultaneously combine the effects of cross sectional area change and friction, cross sectional area change and heat transfer, friction and heat transfer, and all three effects into a single simulation. Moreover, the effects of an unsteady back pressure have also been investigated and the results compared to the steady results. The back pressure varied sinusoidally. Heat addition was applied to the entire flow region in a constant area tube and only to the diverging part of a convergent-divergent nozzle.

The objective of this investigation and its accomplishments are found in section 1. This introduction corresponds to section 2. Section 3 reviews the current literature on the subject including current solutions. The procedure section (4) details the computer code used and its changes, the simulations used to validate the code, and the new steady and unsteady simulations combining more than one effect. Section 5, the results page, details the results of the calculations and simulations while section 6 finishes with concluding remarks.

3. Review of Literature

Variable cross-sectional area, internal wall friction, and heat transfer are common effects that determine compressible flows within a duct for prescribed inlet total energy and density. In addition, the flow also depends on the back pressure. Closed form exact analytical solutions for steady flows exist where only one effect at a time is taken into account and no computational tool is available in the literature to calculate rapidly and directly flows with more than one effect. It is customary to give these solutions as a function of the Mach number and the ratio of specific heats (γ). Pressure, temperature, density, and other properties are usually given as ratios, typically against stagnation properties. Tables have been developed based on such exact solutions. The differential equations for flows determined by more that one effect have been derived, but due to their mathematical complexity, they can only be solved analytically for a very restrictive set of problems. The following equations summarize these solutions.

3.1 Exact Solutions for Changing Cross Sectional Area Only

The flow in a converging or converging-diverging nozzle is isentropic if there are no shocks present and if the flow is adiabatic. This means that the stagnation pressure and temperature remain constant. If a shock is present within an adiabatic flow, then only the stagnation temperature remains constant throughout the flow, whereas the stagnation pressure decreases [4]. Depending on the back pressure and the cross-sectional area variation, the flow inside the nozzle can be subsonic, supersonic, or shocked in the diverging section. If the upstream flow is subsonic and the correct back pressure is present, the flow turns sonic at the exit for a converging nozzle and at the throat for a converging-diverging nozzle. It is important to note that if the flow is subsonic, the Mach number decreases as the area increases and increases as the area decreases. For supersonic flow, the Mach number increases as the area increases and decreases as the area decreases.

Subsonic flow	Supersonic flow
A increases, M decreases	A increases, M increases
A decreases, M increases	A decreases, M decreases

The Mach number (M) and mass flow rate $(\dot{m})$ are given by

$$M = \frac{V_1}{\sqrt{\gamma RT}} \quad \text{And} \quad \dot{m} = \rho AV = \frac{P}{RT} AM\sqrt{\gamma RT} \quad \text{[kg/s]}$$

The pressure ratio (pressure/stagnation pressure) and temperature ratio (temperature/ stagnation temperature) are given by

$$\frac{p_t}{p} = \left(1 + \frac{\gamma - 1}{2} M^2\right)^{\gamma/(\gamma-1)} \quad \text{And} \quad \frac{T_t}{T} = \left(1 + \frac{\gamma - 1}{2} M^2\right)$$

While the cross sectional area of the nozzle versus the throat is given by

$$\frac{A}{A^*} = \frac{\left(\frac{\gamma+1}{2}\right)^{(\gamma+1)/(2-2\gamma)}}{M\left(1+\frac{\gamma-1}{2}M^2\right)^{(\gamma+1)/(2-2\gamma)}}$$

Therefore, given the area ratio at any station along the nozzle axis yields the Mach number and, in turn, pressure and density ratios [4].

3.2 Normal Shock Waves

A normal shock wave is a discontinuity within the flow across which the flow becomes subsonic and static pressure increases, but the stagnation pressure decreases [2]. Normal shocks typically are caused by a higher back pressure than that required to allow the flow to expand isentropically. The region where the normal shock occurs is considered minimal, and therefore, the normal shock is treated as only a discontinuity in the flow. The flow is also considered isentropic before and after the shock, but not from the inlet to the outlet of the nozzle. Isentropic solutions are thus valid before and after the shock, but not across it. It is useful to express the properties of the flow downstream (*state 2*) of the shock in terms of the properties upstream (*state 1*) as illustrated in Figure 1.

The downstream of the shock Mach number (M_2) is given in terms of the upstream Mach number (M_1) by

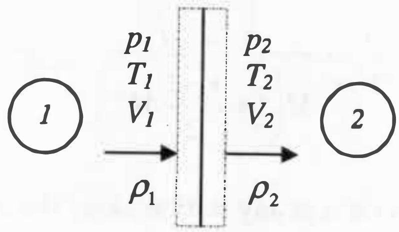

Figure 1. Normal shock control volume.

$$M_2^2 = \frac{M_1^2 + \dfrac{2}{\gamma - 1}}{\dfrac{2\gamma}{\gamma - 1} M_1^2 - 1}$$

Whereas the pressure and temperature ratios are

$$\frac{T_2}{T_1} = \frac{\left(1 + \dfrac{\gamma - 1}{2} M_1^2\right)\left(\dfrac{2\gamma}{\gamma - 1} M_1^2 - 1\right)}{M_1^2\left(\dfrac{2\gamma}{\gamma - 1} + \dfrac{\gamma - 1}{2}\right)} \quad \text{or} \quad \frac{T_2}{T_1} = \frac{\left(1 + \dfrac{\gamma - 1}{2} M_1^2\right)}{\left(1 + \dfrac{\gamma - 1}{2} M_2^2\right)}$$

$$\frac{p_2}{p_1} = \frac{2\gamma M_1^2}{\gamma + 1} - \frac{\gamma - 1}{\gamma + 1}$$

The density and entropy ratios are also given

$$\frac{\rho_2}{\rho 1} = \frac{V_1}{V_2} = \frac{(\gamma - 1) M_1^2}{(\gamma - 1) M_1^2 + 2} \quad \text{And} \quad \frac{s_2 - s_1}{R} = -\ln \frac{p_{t2}}{p_{t1}}$$

Because a normal shock is not isentropic, there is a change in stagnation pressure

$$\frac{p_{t2}}{p_{t1}} = \left[\frac{\frac{\gamma+1}{2}M_1^2}{1+\frac{\gamma-1}{2}M_1^2}\right]^{\gamma/(\gamma-1)} \left[\frac{1}{\frac{2\gamma}{\gamma+1}M_1^2 - \frac{\gamma-1}{\gamma+1}}\right]^{1/(\gamma-1)}$$

3.3 Adiabatic flow in a constant area tube with Friction (Fanno Line Flow)

Adiabatic flow with friction in constant area tube is governed by the length of the tube, the tube's diameter, and the wall friction coefficient. The Mach number and other properties are given in relation to a reference state. The reference state chosen is the sonic state ($M = 1$).

The following equations are integrated between any initial state and a reference state [4].

$$\frac{fL_{max}}{D} = \int_{M=M}^{1} \frac{2(1-M^2)\frac{dM}{M}}{\left(1+\frac{\gamma-1}{2}M^2\right)\gamma M^2} \qquad \text{And} \qquad \int_{p}^{p^*}\frac{dp}{p} = -\int_{M}^{1}\frac{dM}{M}\left[\frac{1+(\gamma-1)M^2}{1+\frac{\gamma-1}{2}M^2}\right]$$

The Mach number increases with the presence of friction only if the flow is subsonic. Wall friction decreases the Mach number if the flow is supersonic. If the flow is subsonic, the flow will be choked at the reference state. It is not possible to accelerate the flow beyond the sonic state. Further increases in the length of the tube will only decrease the mass flow rate.

3.4 Flow in a frictionless constant area tube with heat exchange (Rayleigh Line Flow)

Flow with a constant heat flux changes both stagnation pressure and stagnation temperature. As with flow with friction, the flow properties are expressed in terms of a reference state, denoted by *. The pressure and temperature are given by [4]

$$\frac{p}{p^*} = \frac{1+\gamma}{1+\gamma M^2} \qquad \frac{T}{T^*} = \frac{(1+\gamma)^2 M^2}{\left(1+\gamma M^2\right)^2}$$

The velocity or the inverse of the density ratio is expressed by

$$\frac{V}{V^*} = \frac{\rho^*}{\rho} = \frac{p^*}{p}\frac{T}{T^*} = \frac{(1+\gamma)M^2}{1+\gamma M^2}$$

And the stagnation pressure and temperature

$$\frac{p_t}{p_t^*} = \left[\frac{1+\gamma}{1+\gamma M^2}\right]\left[\frac{1+\frac{\gamma-1}{2}}{1+\frac{\gamma-1}{2}M^2}\right]^{\gamma/(\gamma-1)}$$

$$\frac{T_t}{T_t^*} = \frac{(1+\gamma)^2 M^2}{\left(1+\gamma M^2\right)^2}\frac{\left(1+\frac{\gamma-1}{2}M^2\right)}{\left(1+\frac{\gamma-1}{2}\right)}$$

In a frictionless constant area tube, if the flow is subsonic, the Mach number increases toward *1.0* if the energy flux is positive. If the flow is supersonic, the Mach number decreases to the sonic state. If the flow is choked, increasing the energy flux cannot affect the Mach number, but it will decrease the mass flow rate.

3.5 Flow with more than one effect

As previously stated, closed form analytical solutions do no exist if more than one effect is involved. However, the equations for such flows provide insight into the behavior of the flow.

3.5.1 Flow with Heat Addition and Area Change

The following equation cannot be solved analytically. If the second term can be ignored, then the equation can be solved and the solution to variable area only is obtained.

$$-\frac{dA}{A}+\frac{\left(\gamma M^{2}+1\right)\frac{dq}{c_{p}T}}{2\left(1+\frac{\gamma-1}{2}M^{2}\right)}+\frac{\left(M^{2}-1\right)\frac{dM}{M}}{1+\frac{\gamma-1}{2}M^{2}}=0$$

The sonic points occurs at a position where *dA/A* is positive, or the diverging portion of the nozzle [4].

3.5.2 Adiabatic Flow with Friction and Area Change

$$\frac{1}{2}\gamma M^2 \frac{f}{D} = \frac{1}{A}\frac{dA}{dx} + \frac{dM}{dx}\frac{(1-M^2)/M}{1+\frac{\gamma-1}{2}M^2}$$

"The direct integration of this equation, except for certain specialized cases, is not possible" [4]. Only in the case of *dA/dx = 0* (Fanno flow) or *dM/dx = 0* can this equation be solved analytically.

3.5.3 Flow with Heat Exchange and Friction

Again, it is impossible to solve the governing equations analytically, unless either the heat exchange or friction term in the equation is ignored [2].

$$\frac{\left(1+\gamma M^2\right)\frac{dq}{c_p T}}{2\left(1+\frac{\gamma-1}{2}M^2\right)} + \frac{\gamma M^2 f}{2D_H}dx = \left\{\left(1-\gamma M^2\right) + \frac{\left(1+\gamma M^2\right)}{2}\frac{(\gamma-1)M^2}{1+\frac{\gamma-1}{2}M^2}\right\}\frac{dM}{M}$$

If the Mach number is constant throughout the duct, the right hand side of the equation can be ignored and the equation is solvable. However, the restricted conditions would severely limit the applicability of this model.

Shapiro offered a numerical scheme to solve flows with simultaneously combined friction and heat transfer effects [6]. Shapiro's scheme relied on numerical integrations and algebraically approximations with different parameters for each type of flow. One example from his book [6] was used as a benchmark to validate the generalized algorithm used in this project.

4. Procedure

The algorithm used was generalized to incorporate friction and heat exchange into the simulations. Several benchmarks where the exact solution is known were developed to test the generalized algorithm. The benchmarks are presented here since they are not part of the research for this study and are only used to validate the results from using the generalized algorithm. The results obtained for this project consist of steady simulations incorporating more than one effect as well as unsteady simulations with each effect independently, two combined effects, and all three combined.

This section begins with a brief description of the algorithm, the generalizations introduced, and the validations of such generalizations. The test cases for validation are as follow:

1. Steady supersonic changing cross-sectional area flow with a normal shock.
2. Steady subsonic flow with friction.
3. Steady supersonic flow with friction with a normal shock.
4. Steady subsonic flow with heat exchange.
5. Steady supersonic flow with heat exchange choked at the outlet.
6. Steady subsonic flow with friction and heat exchange.

These are examples where the direct analytical solution exists except benchmark #6, where an approximate numerical solution was offered by Shapiro

[6]. Once the generalization to the algorithm is validated, friction and heat exchange effects are combined into a single simulation. In addition, using a convergent-divergent nozzle, the effect of friction and heat exchange will be briefly evaluated. However, the main focus of this project is to investigate the unsteady flows that result by varying the pressure downstream of the flow. The next steady and unsteady simulations are those developed for part of this project where more than one effect is combined.

7. Steady supersonic flow with friction and heat exchange
8. Steady supersonic flow with area change and/or friction and/or heat exchange.
9. Unsteady supersonic flow in a constant area tube with friction only.
10. Unsteady flow with area change only.
11. Unsteady supersonic flow with changing area and friction only.
12. Unsteady supersonic flow with changing area and heat exchange only.
13. Unsteady flow with area change, friction, and heat exchange.

To compare the unsteady effects, steady simulations with fixed back pressures but with the same run time were also developed. Figure 2 contains an outline of the procedure followed in this project.

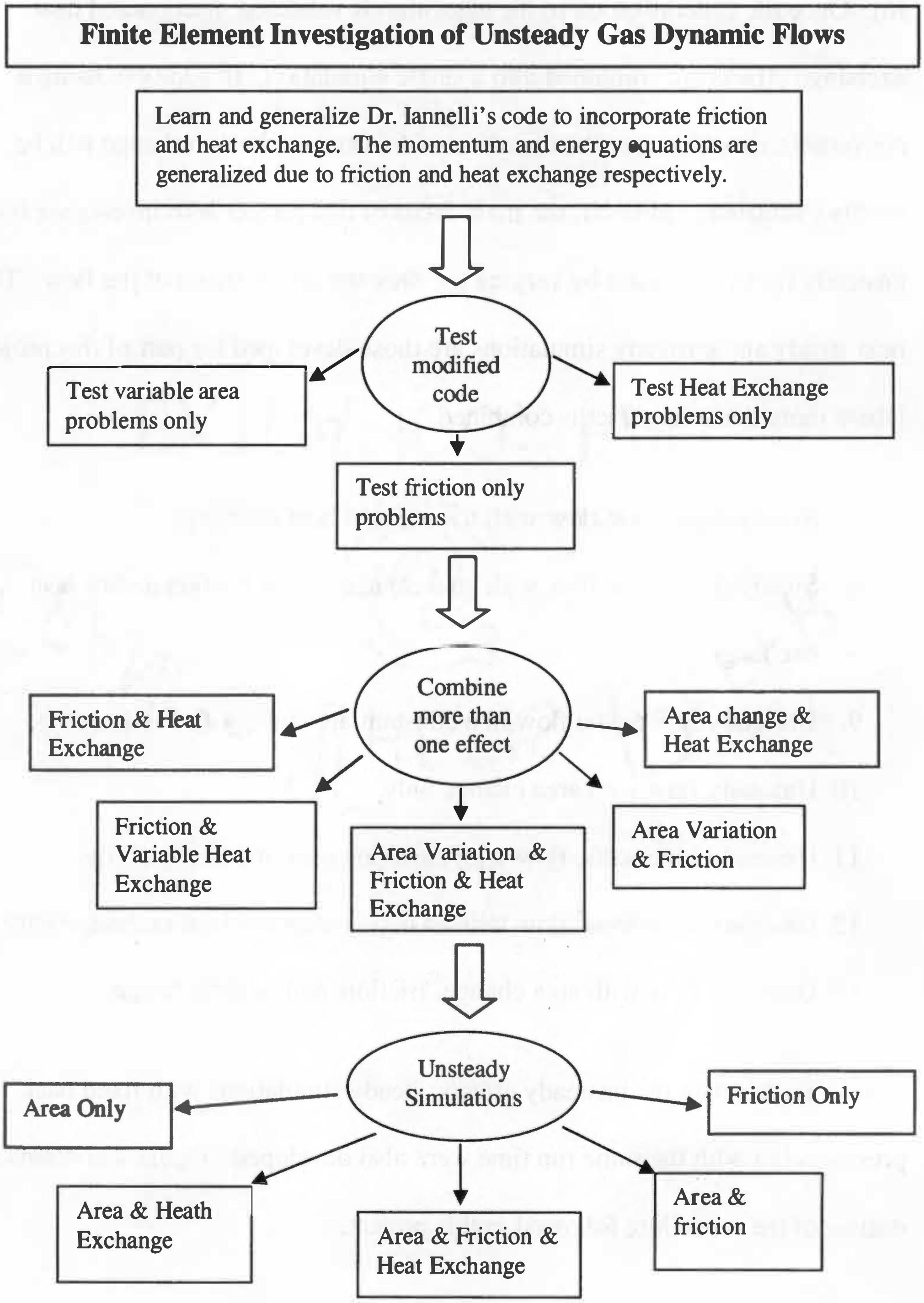

Figure 2. Procedure flow chart

4.1 Description of Computer Code and its Alterations

The baseline code used in this research was developed by Dr. Joe Iannelli. The executive summary of the paper published with the code follows. For a more extensive description of the code, please refer of the original publication [1].

> "...introduces a continuum, i.e. non-discrete, upstream-bias formulation that rests on the physics and mathematics of acoustics and convection. The formulation induces the upstream-bias at the differential equation level, within a characteristics-bias system associated with the Euler equations with general equilibrium equation of state. For low subsonic Mach numbers, this formulation returns a consistent upstream-bias approximation for the non-linear acoustics equations. For supersonic Mach numbers, the formulation smoothly becomes an upstream-bias approximation of the entire Euler flux. With the objectives of minimizing induced artificial diffusion, the formulation non-linearly induces upstream-bias, essentially locally, in regions of solution discontinuities, whereas it decreases the upstream-bias in regions of solution smoothness. The discrete equations originate from a finite element discretization of the characteristic-bias system and are integrated in time within a compact block tridiagonal matrix statement by way of an implicit non-linearly stable Runge-Kutta algorithm for stiff systems. As documented by several computational results that reflect available exact solutions, the acoustics-convection solver induces low artificial diffusion and generates essentially non-oscillatory solutions that automatically preserve a constant enthalpy, as well as smoothness of both enthalpy and mass flux across normal shocks."

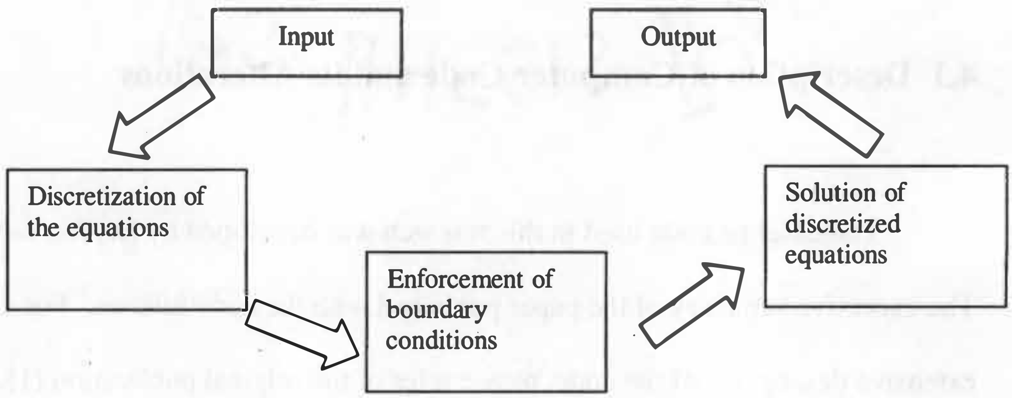

Figure 3. Computer Program flow.

Figure 3 presents a schematic flow chart of the computer program used.

With respect to an inertial reference frame, the quasi-one-dimensional Euler conservation law system is:

$$\frac{\partial q}{\partial t} + \frac{\partial f(q)}{\partial x} = \phi$$

This system consists of the continuity, momentum and total energy equations, and the arrays $q = q(x,t)$, $f = f(q)$ and $\phi = \phi(x,q)$ are defined as

$$q \equiv \begin{Bmatrix} \rho \\ m \\ E \end{Bmatrix}, \qquad f(q) \equiv \begin{Bmatrix} m \\ \dfrac{m^2}{\rho} + p \\ \dfrac{m}{\rho}(E+p) \end{Bmatrix}, \qquad \phi \equiv -\frac{m}{\rho A / A_*} \frac{dA / A_*}{dx} \begin{Bmatrix} \rho \\ m \\ E+p \end{Bmatrix}$$

where ρ is density, p is pressure, m is the volume specific linear momentum (ρu), and E is the volume specific total energy defined as the sum of volume specific internal and kinetic energies $E = \varepsilon + \frac{1}{2}\rho u^2$. For a perfect gas

with $p = \rho RT$, $\varepsilon = \rho c_v T$, $\gamma = \frac{c_p}{c_v}$, and $c_p - c_v = R$, the expression for E becomes

$E = \frac{p}{\gamma - 1} + \frac{1}{2}\rho u^2$. Additionally (A) denotes the duct cross sectional area and (A*) indicates a reference throat area.

Expanding the previous systems gives the continuity, momentum, and energy equations

$$\frac{\partial \rho}{\partial t} + \frac{\partial m}{\partial x} + \frac{m}{\rho A / A_*} \frac{dA / A_*}{dx} = 0$$

$$\frac{\partial m}{\partial t} + \frac{\partial}{\partial x}\left(\frac{m^2}{\rho} + p\right) + \frac{m^2}{\rho A / A_*} \frac{dA / A_*}{dx} = 0 \qquad (1)$$

$$\frac{\partial E}{\partial t} + \frac{\partial}{\partial x}\left(\frac{m}{\rho}(E + p)\right) + \frac{m(E + p)}{\rho A / A_*} \frac{dA / A_*}{dx} = 0$$

These equations do not reflect the effects of friction or heat exchange. The momentum equation was generalized to account for friction effects and the energy equation was generalized to reflect heat exchange. Since these algebraic modifications do not affect the derivatives with respect to time, they are developed from a time-independent analysis for simplicity.

4.1.1 Momentum Equation Additions (Constant Area)

τ_w denotes the wall shear stress in a duct (Figure 4). From a control volume analysis, the momentum equation is

$$\sum F_x = \oint \rho u \vec{V} \cdot \hat{n} dA \tag{2}$$

where $\sum F_x$ denotes the x-component of the total external forces. Expansion of the above equation leads to

$$pA - (p + dp)A - \tau_w A_w = (\rho + d\rho)A(u + du)(u + du) - (\rho uA)u$$

For conservation of mass $(\rho + d\rho)A(u + du) = (\rho uA)$, hence

$$\begin{aligned} pA - (p + dp)A - \tau_w A_w &= (\rho uA)(u + du) - (\rho uA)u \\ pA - Ap - Adp - \tau_w A_w &= (\rho uA)(u) + (\rho uA)du - (\rho uA)(u) \\ -Adp - \tau_w A_w &= (\rho uA)du \end{aligned} \tag{3}$$

Introduce the Hydraulic diameter (D_h) and the parameter *f*.

$$D_h = \frac{4A}{Perimeter} \quad , \quad Perimeter = \frac{4A}{D_h}$$

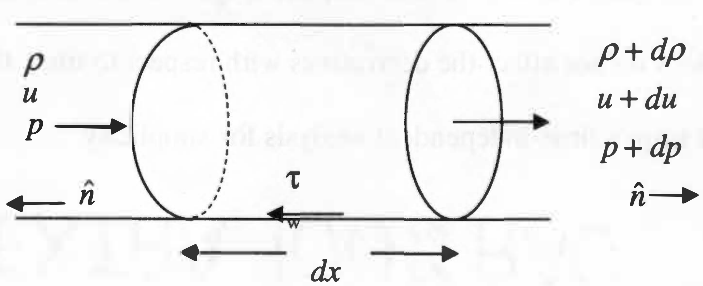

Figure 4. Constant area tube with friction – Control Volume.

$$A_w = (Perimenter)dx$$

$$A_w = \frac{4A}{D_h}dx \tag{4}$$

$$\tau_w = \tfrac{1}{2} f\rho u^2 \tag{5}$$

Substitute (4) and (5) into (3)

$$-Adp - \tfrac{1}{2} f\rho u^2 \frac{4A}{D_h}dx = (\rho u A)du$$

Divide by A and express the differentials dp in terms of derivatives

$$-\frac{dp}{dx} - 2\frac{f\rho u^2}{D_h} = (\rho u)\frac{du}{dx} \quad \text{or with } m = \rho u\text{,} \quad -\frac{dp}{dx} - 2\frac{fm^2}{D_h \rho} = (m)\frac{d}{dx}\left(\frac{m}{\rho}\right) \tag{6}$$

4.1.2 Variable Area

To determine $\tau_w A_w$ in a variable cross-sectional duct (Figure 5), an elementary control volume is considered. This elementary control volume approaches a frustum in which r varies linearly

$$\begin{aligned} dA_w &= \frac{\pi}{\cos\theta}\left[x\frac{dr}{dx} + r\right]dx \\ &= \frac{\pi}{\cos\theta}[x\tan\theta + r]dx \\ &= \frac{\pi}{\cos\theta}\left[x\frac{r}{x} + r\right]dx \end{aligned}$$

$$dA_w = \frac{(2\pi r)dx}{\cos\theta} \tag{7}$$

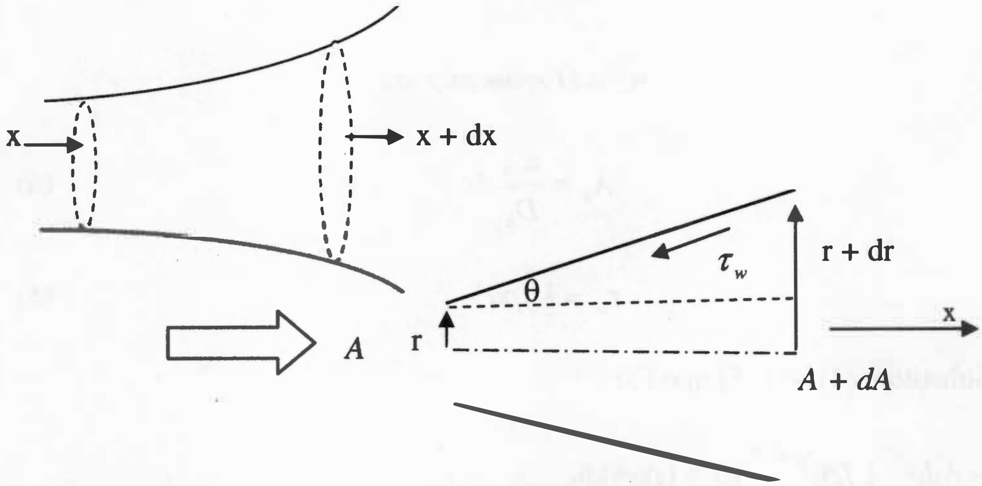

Figure 5. Variable area duct with friction – Control Volume.

The x-component of τ_w becomes $(\tau_w)_x = \tau_w \cos\theta$ and

$$\tau_w \cos\theta(dA_w) = \tau_w \cos\theta \frac{2\pi r dx}{\cos\theta}$$

$$\tau_w \cos\theta(A_w) = \tau_w (2\pi r) dx \tag{8}$$

Which is the same result as in the constant area case.

4.1.3 Energy Equation

Preliminary Derivations

$$c_p - c_v = R \text{ and } \frac{c_p}{c_v} = \gamma \quad \Rightarrow \quad c_v = \frac{c_p}{\gamma}$$

Rearrange E

$$E = \frac{\rho RT}{\gamma - 1} + \frac{\rho u^2}{2}$$

$$c_p\left(1-\frac{1}{\gamma}\right)=R \quad \text{and} \quad c_p\frac{\gamma-1}{\gamma}=R$$

$$E = pT\frac{c_p}{\gamma}+\frac{\rho u^2}{2}$$

$$\therefore \quad \frac{c_p}{\gamma}=\frac{R}{\gamma-1}$$

Rearrange $E + p$

$$E+p=\frac{p}{\gamma-1}+\frac{\rho u^2}{2}+p=\frac{\rho u^2}{2}+\left(\frac{1}{\gamma-1}+1\right)p$$

$$=\frac{\rho u^2}{2}+\frac{1+\gamma-1}{\gamma-1}p=\frac{\rho u^2}{2}+\frac{\gamma}{\gamma-1}p$$

$$=\frac{\rho u^2}{2}+\frac{\gamma}{\gamma-1}R\rho T$$

$$E+p=\frac{\rho u^2}{2}+c_p\rho T$$

Let g denote the energy transfer to the flow per unit time and unit duct length.

The energy equation thus becomes

$$g=\frac{\partial}{\partial x}[uA(E+p)]$$

$$g=\frac{\partial}{\partial x}\left[uA\left(\frac{\rho u^2}{2}+c_p\rho T\right)\right]$$

$$g=\frac{\partial}{\partial x}\left[uA\rho\left(\frac{u^2}{2}+c_pT\right)\right]$$

Expand the differential using the product rule

$$g=\frac{\partial}{\partial x}(uA\rho)\left(\frac{u^2}{2}+c_p\rho T\right)+(uA\rho)\frac{\partial}{\partial x}\left(\frac{u^2}{2}+c_pT\right)$$

However, due to conservation of mass, $\frac{\partial}{\partial x}(uA\rho)=0$ and

$$g = (uA\rho)\frac{\partial}{\partial x}\left(\frac{u^2}{2}+c_pT\right)$$

Divide both sides by $(uA\rho)$

$$\frac{g}{uA\rho} = \frac{\partial}{\partial x}\left(\frac{u^2}{2}+c_pT\right)$$

$$\frac{g}{uA\rho}dx = \frac{\partial}{\partial x}\left(\frac{u^2}{2}+c_pT\right)dx$$

$$\frac{g}{uA\rho}dx = d\left(\frac{u^2}{2}+c_pT\right)$$

Integrate the right hand side

$$\frac{g}{uA\rho}dx = udu + c_pdT$$

In other publications [2], the heat flux differential is defined as

$dq = udu + c_pdT$

Equating the right hand sides of the previous two equations yields

$$dq = \frac{g}{uA\rho}dx \text{ also}$$

$$dq = c_pdT_t = c_p\frac{dT}{dx}dx$$

$$q = \int dq = \int c_p\frac{dT}{dx}dx$$

Therefore

$$q = \int\left(\frac{g}{uA\rho}\right)dx, \quad \frac{dq}{dx} = \frac{g}{uA\rho}$$

and for a constant ratio $\frac{g}{uA\rho}$, the following result is obtained

$$q = \frac{g}{uA\rho}L \quad \text{and} \quad g = q\frac{\rho uA}{L}$$

Therefore $$\frac{\partial}{\partial x}[uA(E+p)] = q\frac{\rho uA}{L}$$

Expand the left hand side by using the product rule of differentiation and $m = \rho u$

$$\frac{\partial}{\partial x}[u(E+p)]A + u(E+p)\frac{\partial A}{\partial x} = q\frac{mA}{L} \tag{9}$$

Find the non-dimensional heat transfer rate. Non dimensional parameters

$$\begin{array}{lll} u = \tilde{u}u_r & p = \tilde{p}p_{st} & \rho = \tilde{\rho}\rho_{st} \\ E = \tilde{E}P_{st} & x = \tilde{x}L & m = \tilde{m}\rho_{st}u_r \end{array}$$

$$\frac{1}{L}\frac{\partial}{\partial x}\left[\tilde{u}u_r\left(\tilde{E}+\tilde{p}\right)p_{st}\right]\frac{A}{A_o} + \tilde{u}u_r\left(\tilde{E}+\tilde{p}\right)p_{st}\frac{1}{L}\frac{\partial A/A_o}{\partial x} = q\frac{\tilde{m}\rho_{st}u_r A/A_o}{L}$$

Divide by A/A_o, *1/L*, u_r, and p_{st}.

$$\frac{\partial}{\partial x}\left[\tilde{u}\left(\tilde{E}+\tilde{p}\right)\right] + \tilde{u}\left(\tilde{E}+\tilde{p}\right)\frac{\partial A/A_o}{A/A_o}\partial x = q\frac{\tilde{m}\rho_{st}}{p_{st}}$$

Therefore

$$\tilde{q} = \frac{q}{\frac{p_{st}}{\rho_{st}}}$$

Adding (6) and (9) results to equations (1) yield the following generalized Euler equations

$$\frac{\partial \rho}{\partial t}+\frac{\partial m}{\partial x}+\frac{m}{\rho A / A_*}\frac{dA / A_*}{dx}=0$$

$$\frac{\partial m}{\partial t}+\frac{\partial}{\partial x}\left(\frac{m^2}{\rho}+p\right)+\frac{m^2}{\rho A / A_*}\frac{dA / A_*}{dx}=\frac{m^2}{\rho}\cdot\frac{2f}{D_h} \tag{13}$$

$$\frac{\partial E}{\partial t}+\frac{\partial}{\partial x}\left(\frac{m}{\rho}(E+p)\right)+\frac{m(E+p)}{\rho A / A_*}\frac{dA / A_*}{dx}=m\cdot q$$

In comparison to the inviscid, adiabatic-flow equations (1), these equations feature the terms $\left(\frac{m^2}{\rho}\cdot\frac{2f}{D_h}\right)$ and $(m\cdot q)$ which specifically model wall friction and heat transfer.

4.2 Benchmarks

The following are solutions to problems where analytical solutions exits or the approximate numerical solution was offered by Shapiro [6]. The accepted results were compared to the results produced by the algorithm. Most of the examples used describe the flow conditions and solve for the exit pressure. While this set of problems is instructional to students, they do not reflect most real world problems where the initial conditions and the back pressure are known. However, they do provide a set of problems to test the modified algorithm. The following are such simulations and the results from the software. Again, such results are presented in this section because they are not part of the research; they are only used to verify an existing code and its alterations.

4.2.1 Steady supersonic shocked flow in a convergent divergent nozzle.

The convergent divergent nozzle is illustrated in Figure 6. This nozzle has a 1.5/1 exit to throat area ratio. With such an area ratio, the nozzle is designed for an exit Mach number of $M = 1.85413$ with a back pressure ratio of $p/p_{01} = 0.16017$. Using this area ratio, a supersonic flow with an embedded normal shock was also modeled. For a back pressure ratio of $p/p_t = 0.700$, a normal shock forms in the diverging part of the nozzle as illustrated in Figure 7

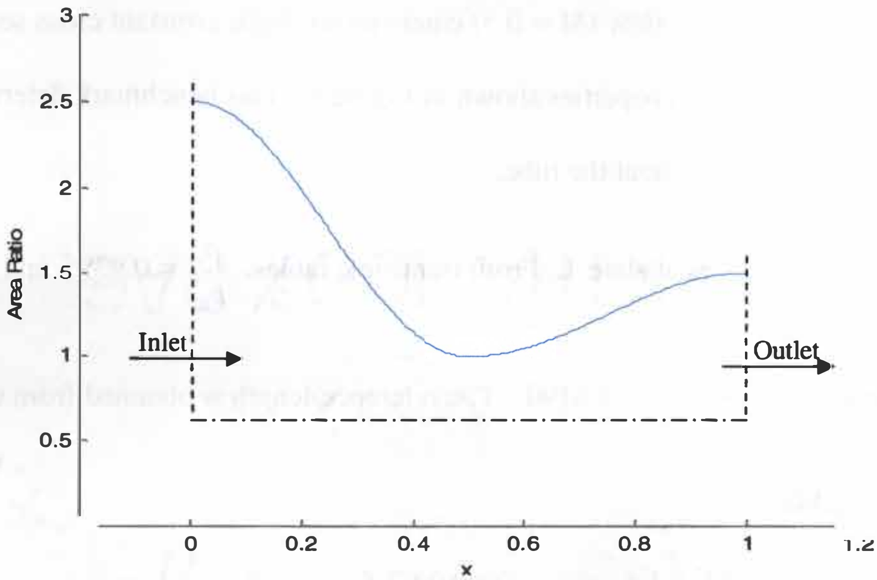

Figure 6. Converging-diverging nozzle. Area Ratio.

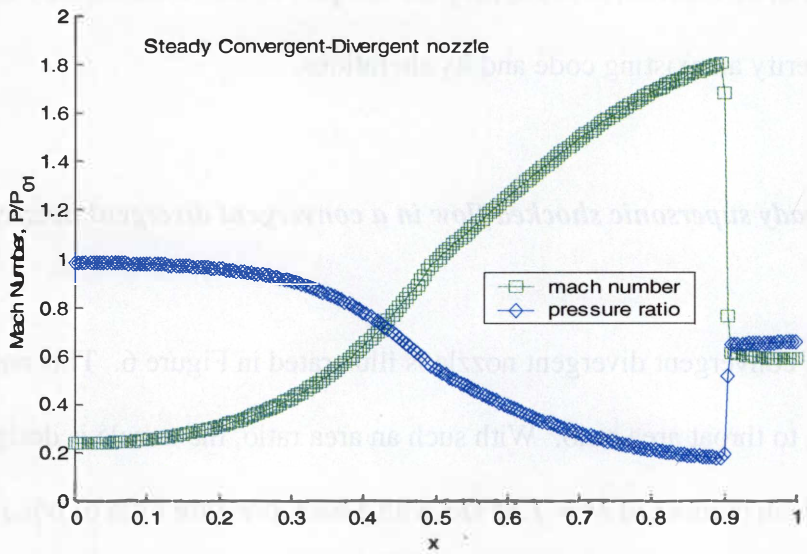

Figure 7. Benchmark - Steady supersonic shocked flow in a convergent divergent nozzle.

4.2.2 Steady subsonic flow with friction.

A subsonic flow ($M = 0.3$) enters an adiabatic constant cross sectional area tube with the properties shown in Figure 8. This benchmark determines the steady flow throughout the tube.

Properties at state 1. From isentropic tables, $\frac{p_1}{p_{01}} = 0.9395$ and from the Fanno line flow, $\frac{p_1}{p^*} = 3.6190$. The reference length is obtained from the Fanno flow tables,

$$\frac{fl_2^*}{D} = \frac{fl_1^*}{D} - \frac{f(l_1^* - l_2^*)}{D} = 5.2992 - \frac{0.02(2.5)}{0.01} = 5.2992 - 5.000$$

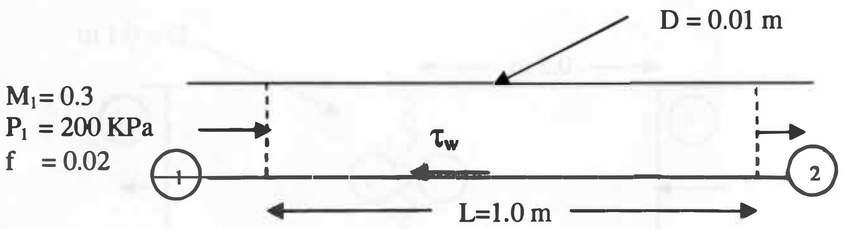

Figure 8. Adiabatic Steady State Constant Area Tube.

$$\frac{fl_2^*}{D} = 0.2992$$

Therefore the Mach number at this location is $M_2 = 0.6595$ and

$\frac{p_2}{p^*} = 1.5932$ and $p_2 = \frac{p_2}{p^*}\frac{p^*}{p_1}p_1 = 88.046$ KPa and $\frac{p_2}{p_{01}} = 0.4136$. The

exit pressure ratio in relation to the inlet stagnation pressure is $\frac{p_2}{p_{01}} = 0.4136$ kPa

4.2.3 Steady Supersonic Flow with Friction and a Normal Shock.

Supersonic flow enters an adiabatic constant area tube. The tube is 1.0 meters in length. A normal shock appears in the middle of the tube. The initial flow properties are as illustrated in Figure 9.

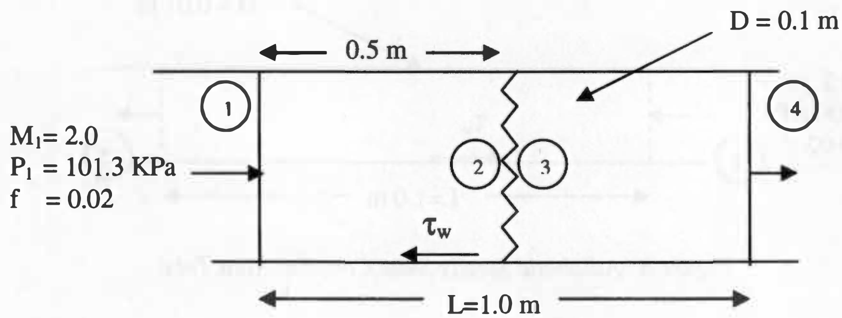

Figure 9. Adiabatic constant area flow with a normal shock.

From the isentropic tables, $\dfrac{p_1}{p_{01}} = 0.1278$ and from the Fanno line flow,

$\dfrac{p_1}{p_t^*} = 0.40825$. It is necessary to determine the physical conditions of the flow before the shock, at state 2. From the Fanno flow tables,

$$\frac{fl_2^*}{D} = \frac{fl_1^*}{D} - \frac{f(l_1^* - l_2^*)}{D} = 0.30499 - \frac{0.02(1.0-0.5)}{0.1} = 0.30499 - 0.100$$

$$\frac{fl_2^*}{D} = 0.20499$$

Therefore the Mach number at this location is $M_2 = 1.6919$ and

$$\frac{p_2}{p_t^*} = 0.5163 \quad \text{and} \quad p_2 = \frac{p_2}{p_t^*}\frac{p_t^*}{p_1}p_1 = 128.112 \text{ KPa}$$

Using the Normal Shock tables with interpolation, and the Fanno flow tables, the flow conditions at state 3 are

$M_3 = 0.6426$

$\frac{p_3}{p_2} = 3.1728$

$p_3 = 406.473$ KPa

$\frac{p_3}{p_t^*} = 1.6385$

$\frac{fl_3^*}{D} = 0.34589$

From the Fanno line tables, calculate the Mach number and other flow conditions at the end of the tube (0.5 meters from the shock location) are as follows

$$\frac{fl_4^*}{D} = \frac{fl_3^*}{D} - \frac{f(l_3^* - l_4^*)}{D} = 0.34586 - \frac{0.02(1.0 - 0.5)}{0.1} = 0.34586 - 0.100$$

$$\frac{fl_4^*}{D} = 0.24586$$

With $\frac{fl_4^*}{D} = 0.24586$, $M_4 = 0.68182$ and $\frac{p_4}{p_t^*} = 1.53688$. Therefore, the back pressure is

$$p_4 = \frac{p_4}{p_t^*}\frac{p_t^*}{p_3} p_3 = 381.259 \text{ KPa}$$

and

$$\frac{p_4}{p_{01}} = p_4 \frac{p_1}{p_{01}} \frac{1}{p_1} = 0.48101$$

Therefore, using the $\frac{p_4}{p_{01}}$ ratio, the friction coefficient, the tube dimensions, and the initial conditions, the software gave the results in Figure 10. The algorithm correctly calculated the position of the shock and the exit properties.

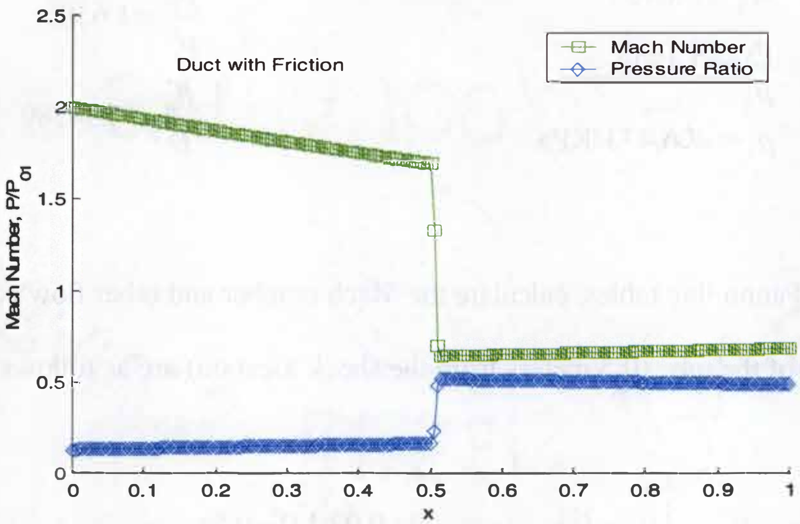

Figure 10. Benchmark - Steady supersonic shocked flow in a constant area duct.

4.2.4 Steady Subsonic Flow with Heat Transfer

A subsonic flow enters a frictionless, constant area tube with energy added at a rate of *50.0 kJ/Kg* of air (Figure 11). The exit properties are required.

From isentropic tables, for M_1, $= 0.20$, $T/T_{01} = 0.9921$, therefore, the stagnation temperature and pressure are

$$T_{01} = \frac{300}{0.9921} = 302.4K \qquad \text{and} \qquad p_{01} = p_1 \frac{p_{ti}}{p_1} = \frac{100}{0.9725} = 102.8kPa$$ The

difference in stagnation temperature between two points in Raleigh flow is given by

$$T_{02} - T_{01} = \frac{q}{c_p} = \frac{50kJ/kg}{1.004kJ/kg \cdot K} = 49.8K$$ and, therefore $T_{02} = 349.8$ K.

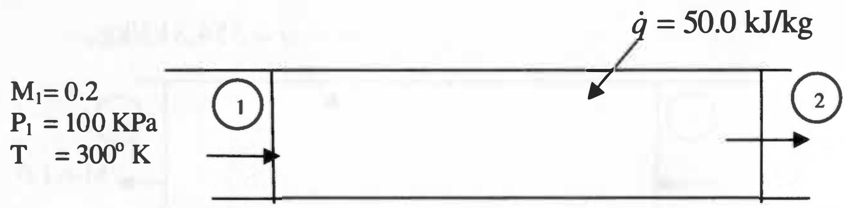

Figure 11. Frictionless constant area tube with subsonic flow & heat exchange.

From Raleigh flow tables,

$$T_2 = \frac{T_2}{T^*}\frac{T^*}{T_1}T_1 = (0.2387)\frac{1}{0.2066}300 = 346.6K$$

and

$$p_2 = \frac{p_2}{p^*}\frac{p^*}{p_1}p_1 = (2.252)\frac{1}{2.273}100 = 99.1kPa$$

The exit pressure in relation to the inlet stagnation pressure is

$$\frac{p_2}{P_{01}} = \frac{99.1}{102.8} = 0.9640$$

4.2.5 Steady Supersonic Flow with Heat Transfer.

A supersonic flow enters a frictionless constant area tube as illustrated in Figure 12. The flow at the outlet is choked when 354.3 kJ/kg of energy are added. Outlet flow properties are required.

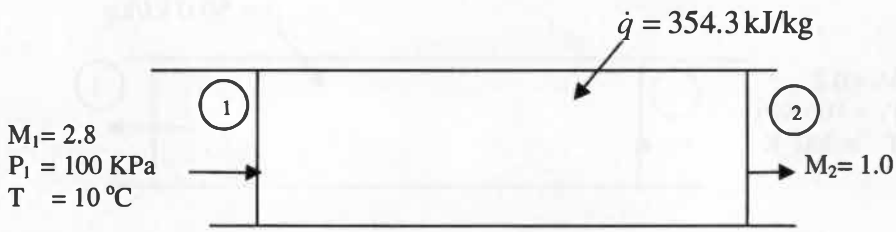

Figure 12. Supersonic flow in a frictionless constant area tube with chocked flow at the outlet.

Properties at state 1.

From the isentropic tables, $\frac{p_1}{p_{01}} = 0.03684$ and from the Rayleigh line flow,

$\frac{p_1}{p^*} = 0.20040$. For the flow to be choked at the outlet, state 2 is also the * state

$$\text{and } T_{02} = T_0^* \text{ and } p_2 = p^* = \frac{p^*}{p_1} p_1 = 499.0 \text{ kPa}\text{, therefore}$$

$$\frac{p_2}{p_{01}} = p_2 \frac{p_1}{p_{01}} \frac{1}{p_1} = 0.18387$$

Using the resulting back pressure ratio, and the initial conditions, the resulting flow was generated in Figure 13 where the correct exit Mach number is calculated.

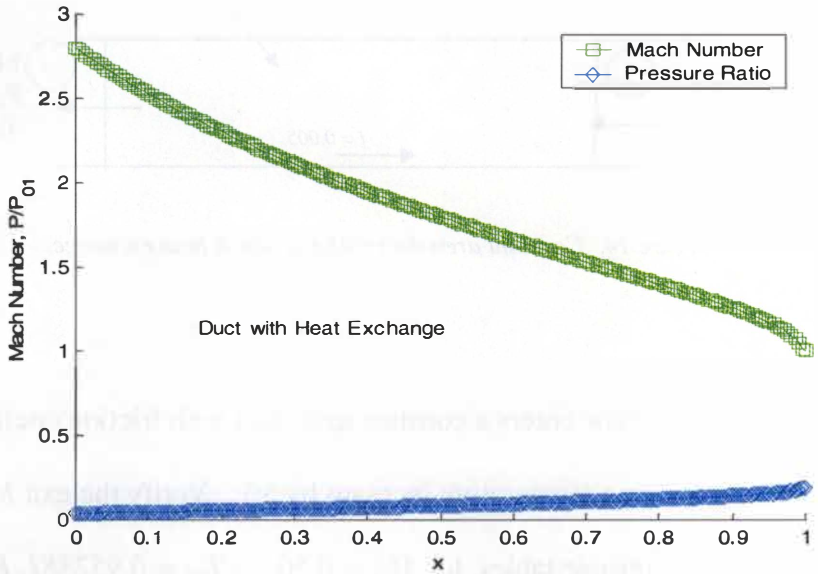

Figure 13. Benchmark - Steady supersonic shocked flow, constant area with heat transfer.

4.2.6 Steady Subsonic Flow with Friction & Heat Transfer

This benchmark essentially coincides with an example problem in Shapiro [6]. In that reference, the problem was solved through a trial and error procedure resulting in the calculation of several intermediate parameters. Furthermore those calculations only determined the outlet Mach number and pressure ratio. The generalized algorithm in this thesis, instead, directly solved the problem and provided not only outlet mach number and pressure ratio, but all flow variables throughout the duct. The results so generated for the outlet Mach number and pressure ratio agree with Shapiro's results.

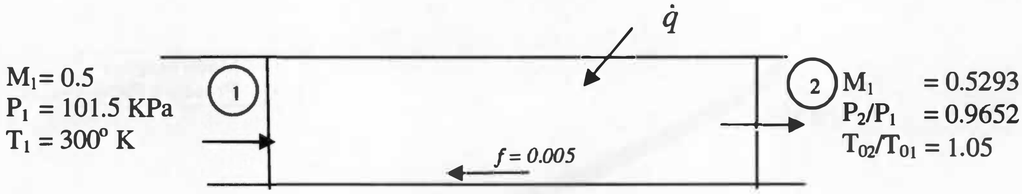

Figure 14. Constant area duct with friction & heat exchange.

A subsonic flow enters a constant area duct with friction coefficient $f = 0.005$ and a stagnation temperature increase by 5%. Verify the exit Mach number. From isentropic tables, for $M_1 = 0.50$, $T_1/T_{01} = 0.952381$, $P_1/P_{01} = 0.84302$, therefore, the stagnation temperature and pressure are

$$T_{01} = \frac{300K}{0.952381} = 315.0K \quad \text{and} \quad p_{01} = p_1 \frac{p_{01}}{p_1} = \frac{101.5kPa}{0.84302} = 120.4kPa$$

The constant heat flux is determined by the difference in stagnation temperature between the inlet and outlet

$$q = c_p(T_{02} - T_{01}) = c_p \frac{(T_{02} - T_{01})}{T_{01}} T_{01}$$

$$q = c_p(1.05 - 1)T_{01}$$

$$q = (1.004kJ/kg \cdot K)(0.05)(315.0K) = 15.813kJ/kg$$

$$q = 15.813kJ/kg$$

non-dimensionalize the heat flux by $\tilde{q} = \dfrac{q}{R_{air}T_{01}} = \dfrac{15.813kJ/kg}{(0.287kJ/kg \cdot K)(315.0K)}$

$$\tilde{q} = 0.1749$$

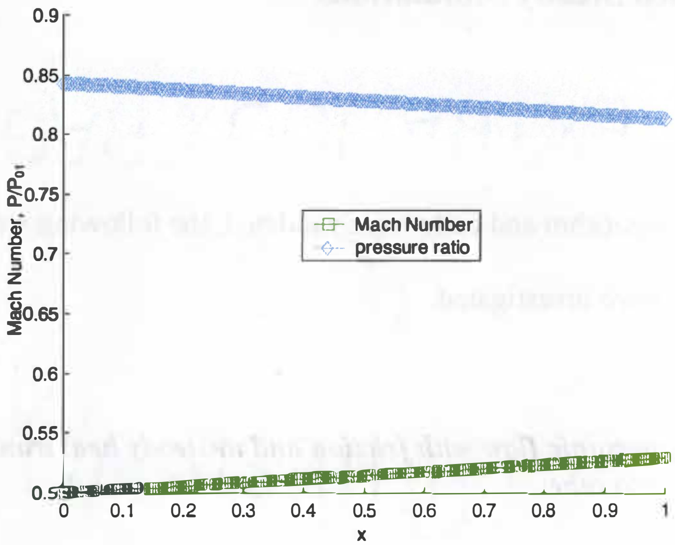

Figure 15. Mach number and pressure ratio in a constant area duct with friction and heat transfer.

The exit pressure ratio is given by

$$\frac{p_2}{P_{01}} = \frac{p_1}{p_{01}}\frac{p_2}{p_1} = (0.9652)(0.84302) = 0.8137$$

Using these boundary conditions, the results in Figure 15 were obtained. Table 1 thus shows that the generalized algorithm solution agrees with Shapiro's results. This solution was generated directly.

Table 1. Benchmark results and comparison to Shapiro's Results.

	Generalized Algorithm	Shapiro
Exit Mach Number:	0.5296	0.5293
Exit Pressure Ratio	0.8138	0.8137
Exit Temperature ratio:	0.9939	
Inlet speed ratio:	0.5778	
Exit speed ratio:	0.6248	

4.3 Combined Steady Simulations

Once the algorithm and code were validated, the following steady and unsteady flows were investigated.

4.3.1 Steady supersonic flow with friction and unsteady heat transfer in a constant area tube.

This is the same flow scenario as the supersonic flow with friction only. Without any heat exchange, a normal shock appears in the middle of the tube as illustrated in Figure 16. The heat transfer rate ratio is varied linearly between *-0.25* to *0.10*. This will assure the shock will remain inside the tube.

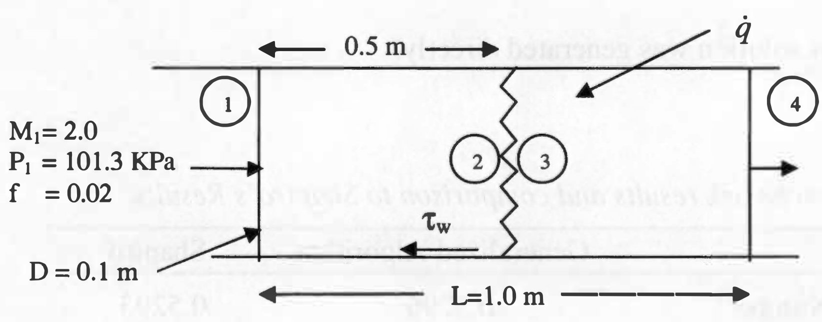

Figure 16. Constant area supersonic flow with friction & Heat Exchange

4.3.2 Steady flow in a convergent divergent nozzle with friction and heat transfer.

The friction and heat exchange effects on flow were combined in the previous simulation. The following simulations will combine friction and/or heat exchange with a converging diverging nozzle.

- Steady and unsteady flow with variable cross sectional only
- Steady and unsteady flow with variable cross sectional area and friction
- Steady and unsteady flow with variable cross sectional area and heat exchange
- Steady and unsteady flow with variable cross sectional area, friction, and heat exchange

Figure 17 represents the addition of friction and heat exchange in the converging diverging nozzle. While friction acts throughout the nozzle, a constant steady heat flux is applied only to the diverging part of the nozzle. This is done because the nozzle is choked at the throat. The back pressure is fixed at $P_b/P_{01} = 0.7, f = 0.005$, and $\dot{q} = 1$. Without friction or heat transfer, these conditions generate the benchmark case in section 4.2.1. The heat transfer ratio is defined as $\dot{q} = \dfrac{q}{\dfrac{p_{tot(in)}}{\rho_{tot(in)}}} = \dfrac{q}{R_{air}T_{tot(in)}}$. The change in stagnation temperature is

therefore

$$T_{tot(out)} - T_{tot(in)} = \frac{q}{c_p} = \frac{R_{air} T_{tot(in)}}{c_p} \dot{q}.$$

Divide by the inlet stagnation temperature and

$$\frac{T_{tot(out)}}{T_{tot(in)}} - 1 = \frac{R_{air}}{c_p} \dot{q}$$

$\frac{T_{tot(out)}}{T_{tot(in)}} = 1.286$. Therefore, $\dot{q} = 1$ increases the stagnation temperature by 28.6%.

4.4 Unsteady Flows

For the unsteady simulations, a constant area tube and a converging diverging nozzle are used. For the constant area tube, the case described in

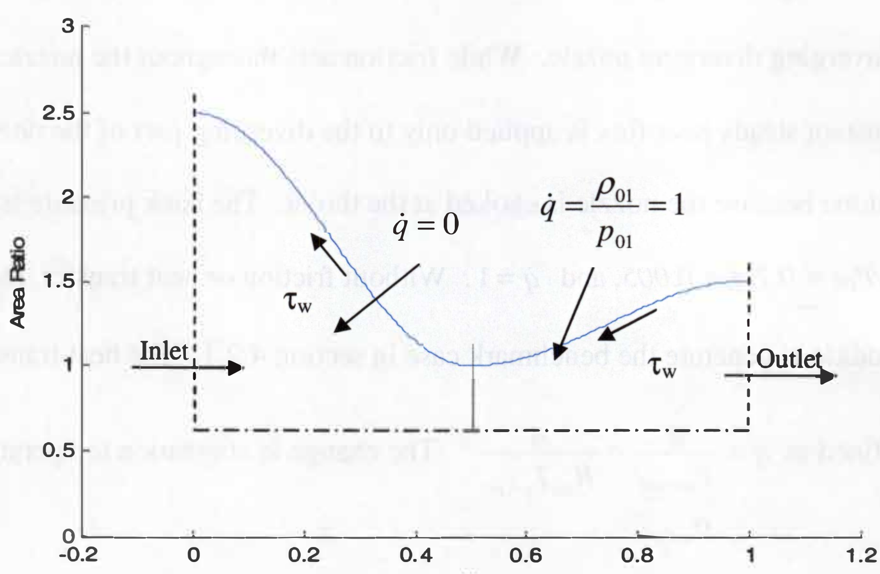

Figure 17. Variation of area ratio with friction - Diagram

section 4.2.3 was used. It is supersonic flow with a normal shock standing in the middle of the tube. For the unsteady simulation in the convergent-divergent nozzle, the cases described in section 4.3.2 were used.

4.4.1 Unsteady supersonic flow with friction and heat exchange in a constant area tube.

Using the previous simulation's scenario, the back pressure is varied sinusoidally (Figure 18). It was determined that a range of back pressure ratios between *0.4610* and *0.5010* confined the normal shock within the duct. Using this range, the following cosine function for the back pressure was developed:

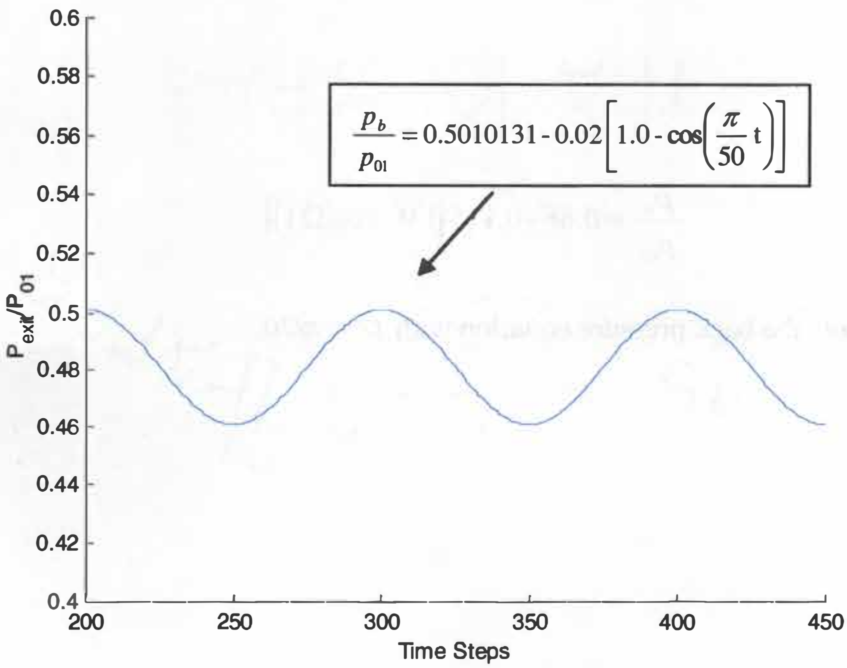

Figure 18. Unsteady back pressure ratio for constant area tube with friction

$$\frac{p_b}{p_{01}} = 0.5010131 - 0.02\,[1.0 - \cos(\Omega\, t)]$$

where Ω is any frequency. For this project, *Ω = π/50*. For this flow, the algorithm converged toward a steady solution in *200* time of numerical integration steps.

4.4.2 Unsteady flow in a converging-diverging nozzle with friction and heat transfer.

Four simulations in a converging diverging nozzle were developed. The range of back pressures varies between *0.65* and *0.88*. The range ensures that the shock is contained in the diverging portion of the nozzle if no friction or heat exchange effects are added. For this case, the back pressure equation is as follows:

$$\frac{p_b}{p_{01}} = 0.88 - 0.115\,[1.0 - \cos(\Omega\, t)]$$

Figure 19 plots the back pressure equation with *Ω = π/20*.

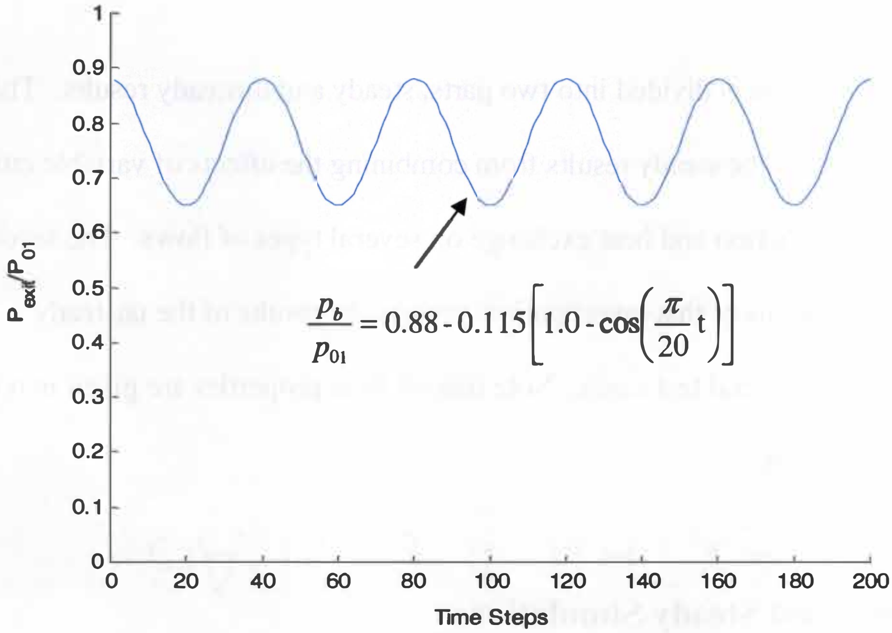

Figure 19. Unsteady back pressure for converging-diverging nozzle.

5. Results

This section is divided into two parts, steady and unsteady results. The first part analyses the steady results from combining the effects of variable cross-sectional area, friction and heat exchange on several types of flows. The second part, the main focus of this investigation, reports the results of the unsteady simulations for several test cases. Note that all flow properties are given in non-dimensional terms.

5.1 Combined Steady Simulations

Four different flow combinations were considered and analyzed. The first, using a constant area tube, combined the effects of friction and heat exchange. For the other three, the effects of friction only, heat exchange only, and the combination of friction and heat exchange were added to a flow in a converging-diverging nozzle.

5.1.1 Constant area tube with friction and heat exchange.

The type of flow chosen had a supersonic inlet with $M = 2.0$ and a fixed back pressure ratio $P_b/P_{01} = 0.48101$. Without any heat exchange, a normal shock appeared in the middle of the *1.0 m* tube. Then, heat exchange coefficient ($\dot{q}$) was varied linearly as a ratio

$$-0.25 \le \frac{\dot{q}}{R_{air}T_{tot(in)}} = \frac{\dot{q}}{\dfrac{p_{tot(in)}}{\rho_{tot(in)}}} \le 0.10$$

This range was chosen because it confined the normal shock inside the tube. As it can be seen in the progression in Figure 20, the shock tended to move toward the outlet if the flow was cooled and toward the inlet if the flow was heated.

The results are consistent with the theory. Heating tends to increase the Mach number for subsonic flow while it decreases it if the flow is supersonic. Since the shock is present for every heat flux value, the flow at the outlet is subsonic and the back pressure is fixed. When there is no heat flux, the shock occurs at the middle and, due to friction, the Mach number is raised and the pressure is lowered to the back pressure in the remainder of the tube. When heat is added, heating tends to have the same effect as friction; therefore, the shock occurs more and more upstream so that the pressure decreases to the back pressure over a longer tube section. The opposite is true when cooling occurs. After the shock, the pressure is closer in value to the back pressure and therefore pressure adjusts to the back pressure over a shorter tube length. This effect is seen in Figure 21.

Selected pressure curves were plotted as continuous functions for clarity. The inlet pressure *(~0.13)* increased until the shock formed. After the shock, the

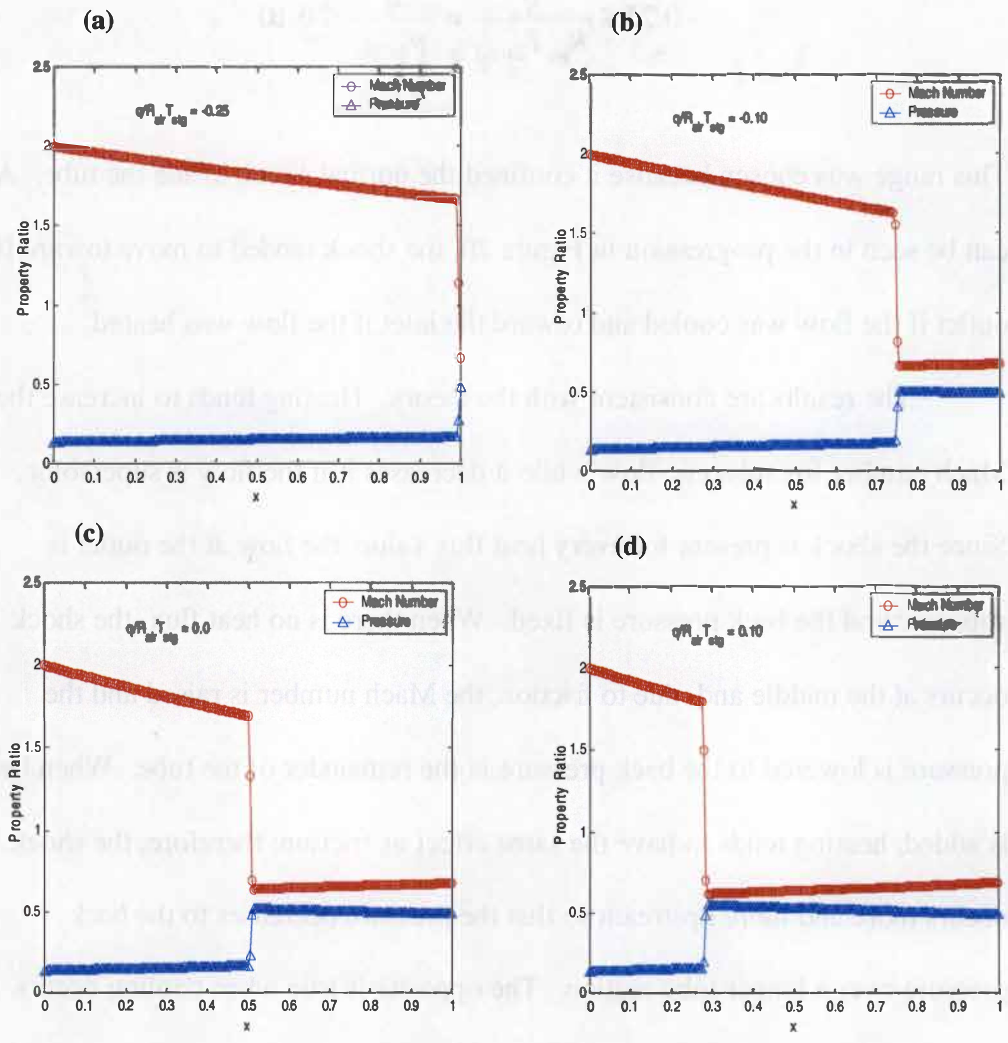

Figure 20. Constant area tube with friction and varying heat flux ratio at (a) -0.25, (b) 0.10, (c) 0.0, (d) 0.10.

flow was subsonic and the pressure decreased toward the back pressure (P_b = *0.48101*). It is not the intention of the author to give a universal relationship between friction and heat transfer, but only to demonstrate the capabilities of the generalized algorithm. However, for this particular case, there was a strong correlation between heat flux and exit velocity. From Figure 22, the exit velocity increased linearly as the heat flux increased. This correlation does not hold if the shock was already at the outlet of the tube, which was the case for heating ratios lowered than *-0.20*. The equation for the line describing the exit velocity pattern is $y = 0.2029x + 0.7717$

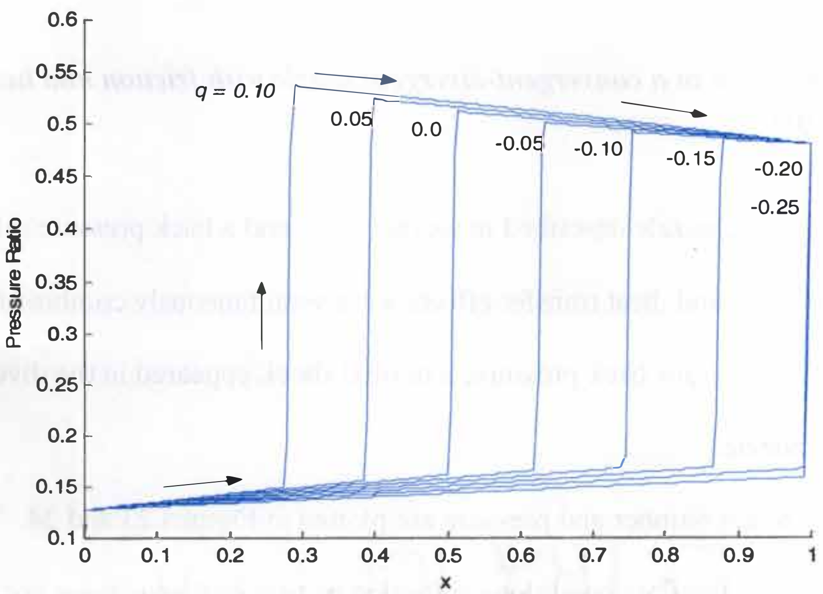

Figure 21. Pressure in a constant area tube with friction and variable heat flux.

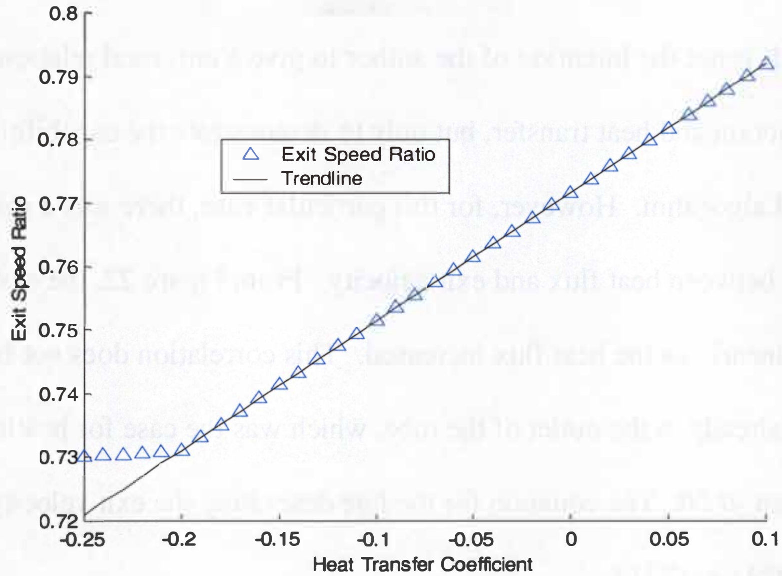

Figure 22. Exit speed in a constant area tube with varying heat transfer.

5.1.2 Steady flow in a convergent-divergent nozzle with friction and heat transfer.

Using the nozzle described in section 4.2.2 and a back pressure ratio of *0.7*, both friction and heat transfer effects were simultaneously combined into the simulation. Using this back pressure, a normal shock appeared in the divergent part of the nozzle.

The Mach number and pressure are plotted in Figures 23 and 24. The red curves represent the flow conditions if friction or heat exchange were not present. The blue curves represent the added effect of friction while the green curves represent the effect of heat exchange. The yellow curves show the results under both effects. Because the back pressure is fixed, the exit pressure for all cases is the same. The exit Mach number is not the same however, neither is the exit density as seen in Figure 25. The exit density of the flow is lower when there is a heat flux.

Figure 26 shows the velocity profile. Because of supersonic heating, ($\sim 0.5 < x < 0.75$) the velocity decreases. After the shock, the flow was subsonic and the velocity increases. The following table compares selected results from all four test cases.

The exact location where the flow is sonic is not known, however, the location is between the values indicated in Table 2. The plus (+) sign by some of the sonic locations indicate that the flow is sonic closer to the second x-location. When fiction and/or heat transfer are present, the nozzle is no longer choked at the throat but in the diverging section [4].

Table 2. Exit Speed and Exit Mach number.

Effect	Exit speed	Exit Mach #	Mach 1.0 x-location
Area Only	0.6297	0.5491	0.500 - 0.505
Area, Friction	0.6289	0.5483	+ 0.500 - 0.505
Area, Heat Ex.	0.7103	0.5814	0.535 - 0.540
Area, Friction, Heat Ex.	0.7092	0.5804	+ 0.535 - 0.540

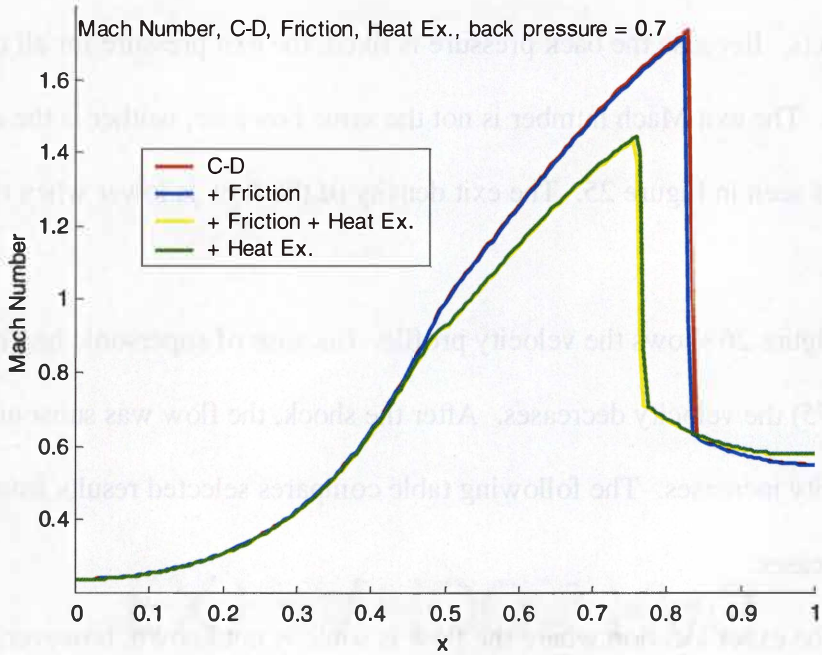

Figure 23. Mach Number in a C-D nozzle with friction and heat transfer.

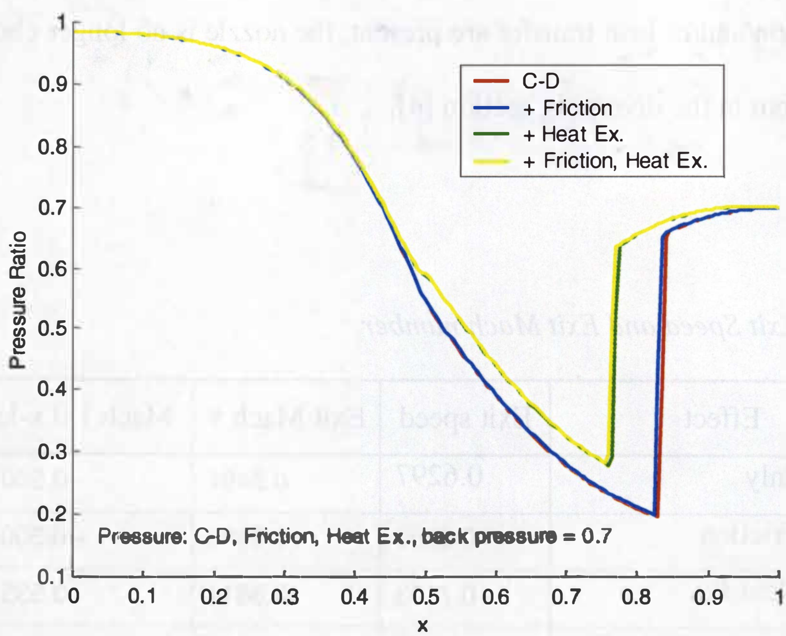

Figure 24. Pressure ratio in a C-D nozzle with friction and heat transfer.

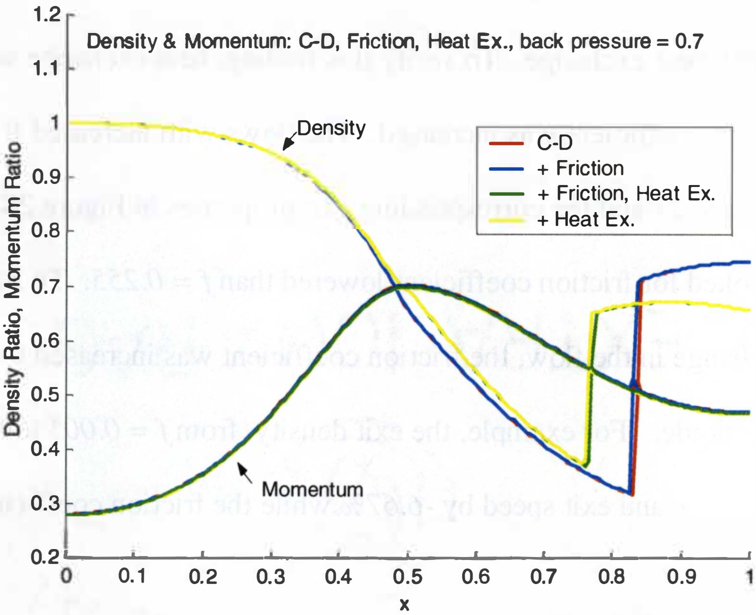

Figure 25. Momentum in a C-D nozzle with friction and heat transfer.

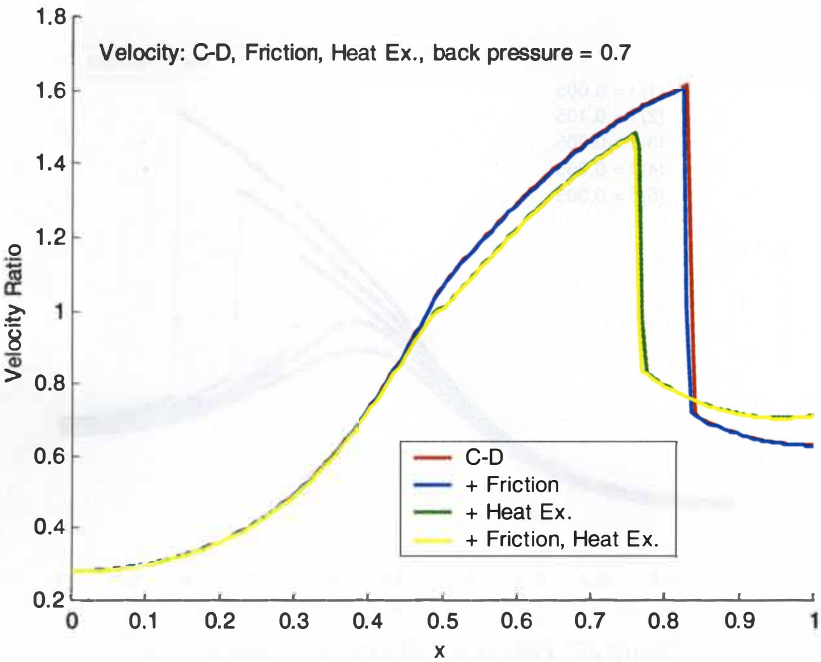

Figure 26. Speed in a C-D nozzle with friction and heat transfer.

Friction did not change the flow conditions significantly, both by itself or combined with heat exchange. To verify this finding, heat exchange was removed and the friction coefficient was increased. The flows with increased friction are plotted in Figure 27 and the corresponding exit properties in Figure 28. The flow remained choked for friction coefficient lowered than $f = 0.255$. To make a significant change in the flow, the friction coefficient was increased by at least an order of magnitude. For example, the exit density, from $f = 0.005$ to 0.255 change by *-0.81%* and exit speed by *-6.67%* while the friction coefficient change by *-5,000%*.

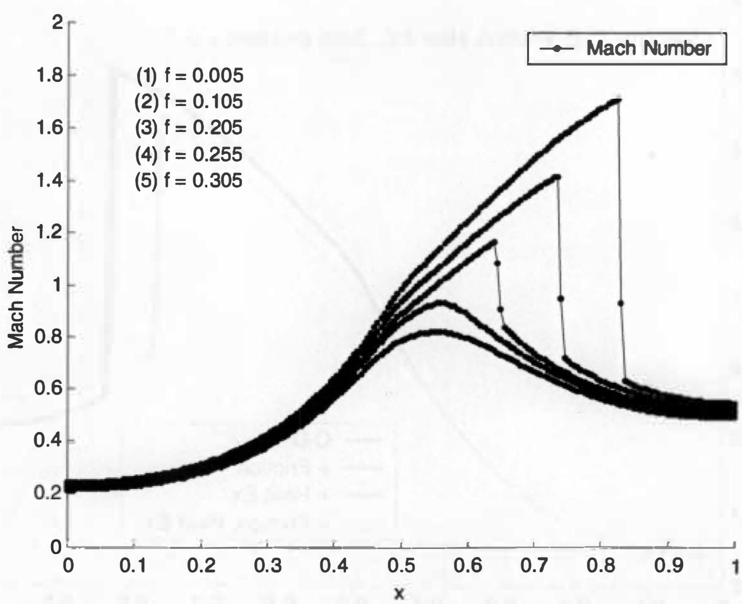

Figure 27. Flow in a C-D with increasing friction.

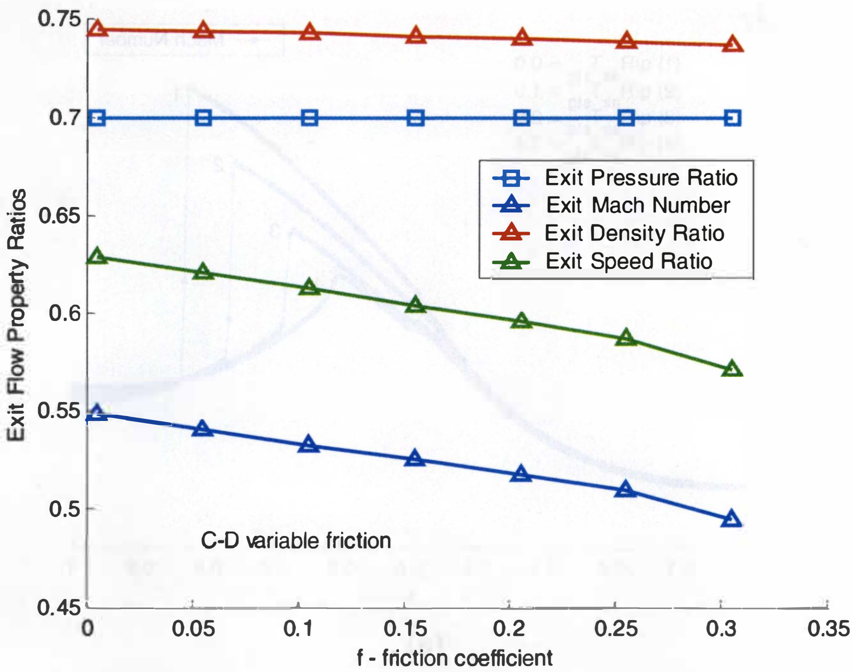

Figure 28. Exit properties for flow in a C-D with increasing friction.

While normal friction estimates had little effect on this particular flow, the opposite is true for heat exchange. For the heat flux chosen, $\tilde{q} = 1.0$ (~85.6 kJ/kg air), it can be seen that heat transfer had a major impact in the flow. Figure 29 shows the flow with increasing heat flux. For a 100% increase in heat flux (from $\tilde{q} = 1.0 - 2.0$), exit density change was -10.61% and the exit speed change was 10.22%. Figure 29 (b) shows a change in Mach number at x = 0.5. This is due to the heat flux only acting in the diverging part of the nozzle and therefore there is an abrupt change in the flow at this location. Figure 30 shows the exit properties with increasing heat flux.

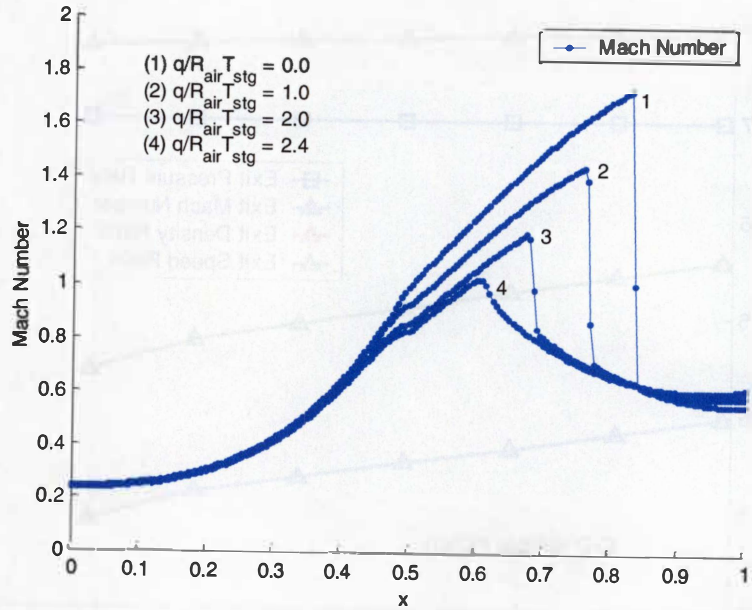

(a)

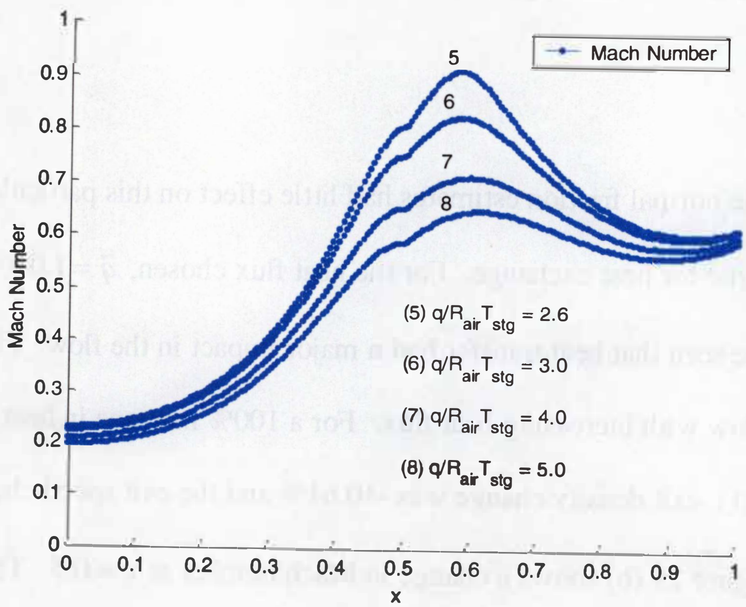

(b)

Figure 29. Flow in a C-D nozzle with increasing heat transfer: (a) choked flow, (b) subsonic flow.

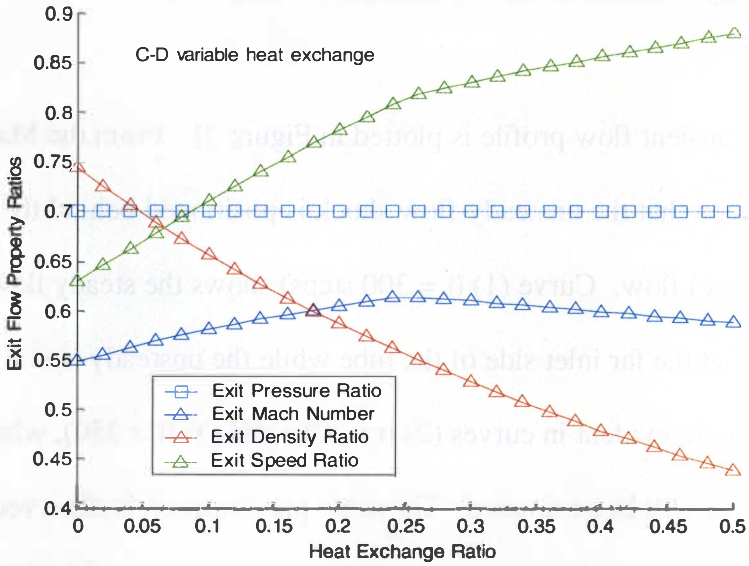

Figure 30. Exit properties for flow in a C-D with increasing heat transfer.

5.2 Unsteady Simulations

The results of five unsteady flows are presented. The first is adiabatic flow in a constant area tube with friction. The other unsteady simulations deal with flows within a convergent divergent nozzle with the effect of friction and/or heat exchange combined. For all cases, two types of results are given. The first is an illustration of the changing flow inside the nozzle as the back pressure changes. For each flow property, the unsteady flow curves are accompanied by a corresponding steady case. The other results are selected exit properties for each time step.

5.2.1 Unsteady constant area, adiabatic flow with friction.

The transient flow profile is plotted in Figure 31. From the Mach number curves, it is seen that the unsteady-flow shock is positioned behind the steady (solid black line) flow. Curve (1) (t = 300 steps) shows the steady flow with its normal shock at the far inlet side of the tube while the unsteady is still moving left. This is more evident in curves (2) (t = 330) and (3) (t = 350), where (3) is as far as the shock will be positioned. The same phenomenon is observed for the pressure, density, and temperature plots in Figures 32, 33, and 34. This is due to the inertia in the changing unsteady flow.

For a time dependent periodic back pressure, an important question was to determine whether the other exit properties would exhibit the same frequency.

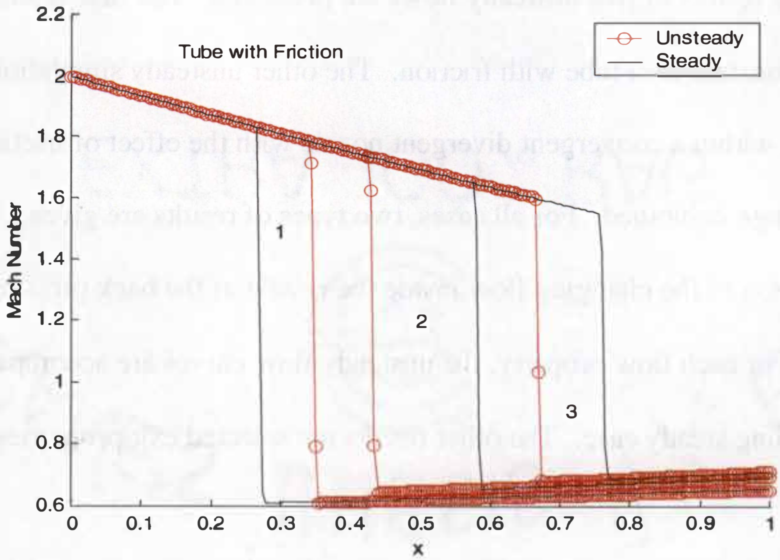

Figure 31. Unsteady constant area, adiabatic flow with friction – Mach Number.

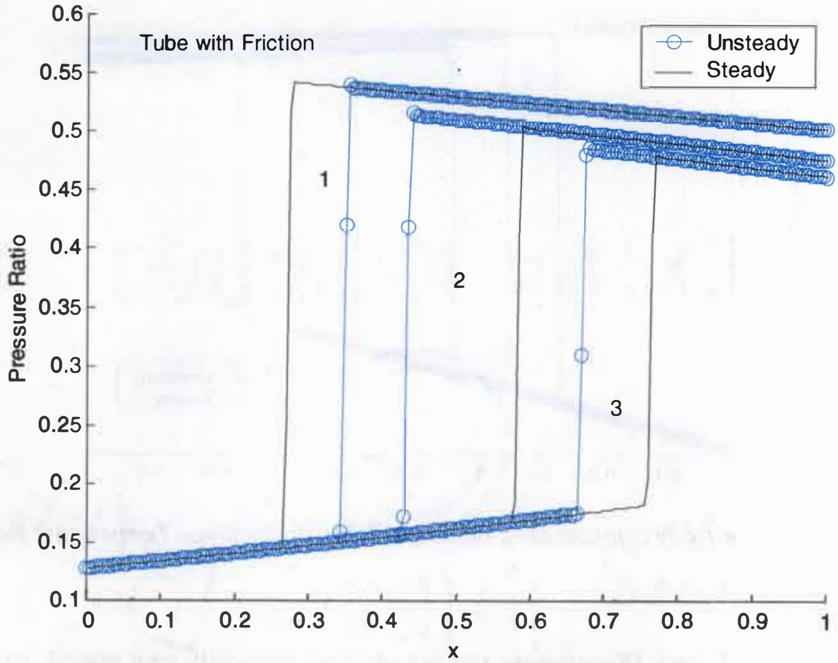

Figure 32. Unsteady constant area, adiabatic flow with friction – Pressure Ratio.

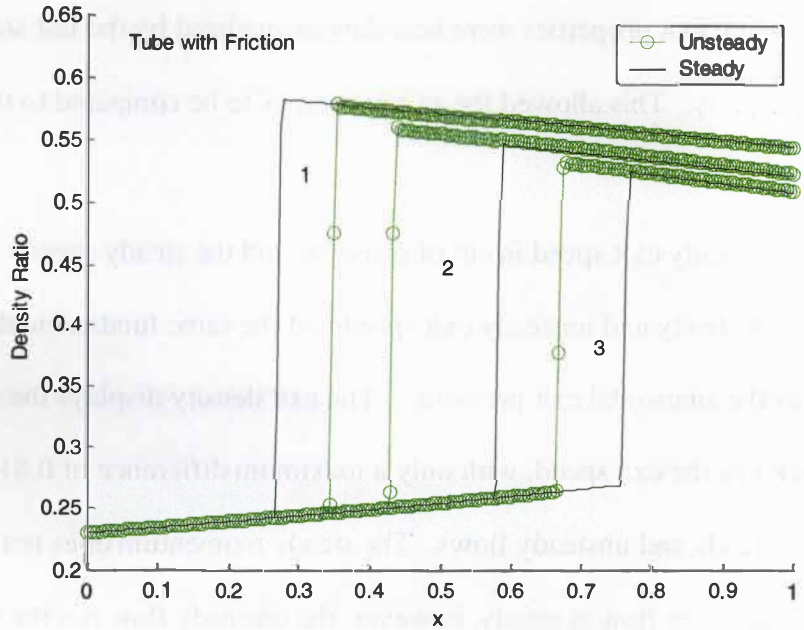

Figure 33. Unsteady constant area, adiabatic flow with friction – Density Ratio.

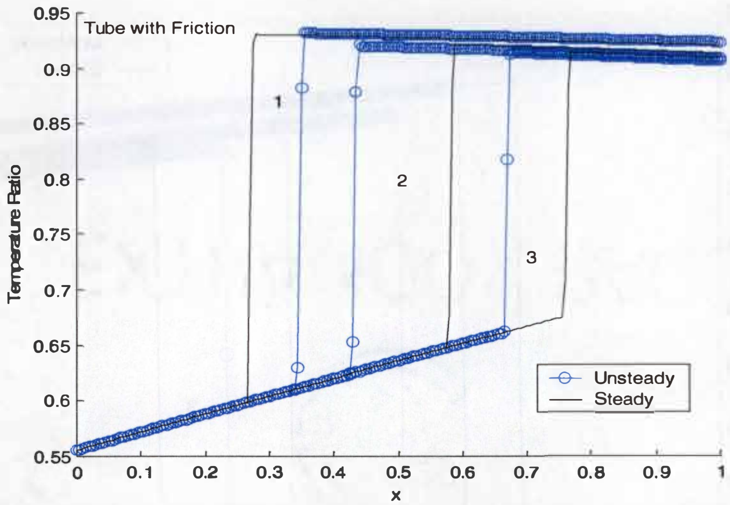

Figure 34. Unsteady constant area, adiabatic flow with friction – Temperature Ratio.

Figures 35, 36, 37, and 38 compare the steady and unsteady exit speed, exit density, exit momentum, and exit temperature with the exit pressure. The magnitudes of all exit properties were non-dimensionalized by the last step of the respective property. This allowed the exit properties to be compared to the back pressure.

The unsteady exit speed is out of phase behind the steady speed. However, both steady and unsteady exit speed had the same fundamental frequency as the sinusoidal exit pressure. The exit density displays the same characteristics as the exit speed, with only a maximum difference of 0.81% between the steady and unsteady flows. The steady momentum does not change, as expected since the flow is steady, however, the unsteady flow has the same period as the pressure.

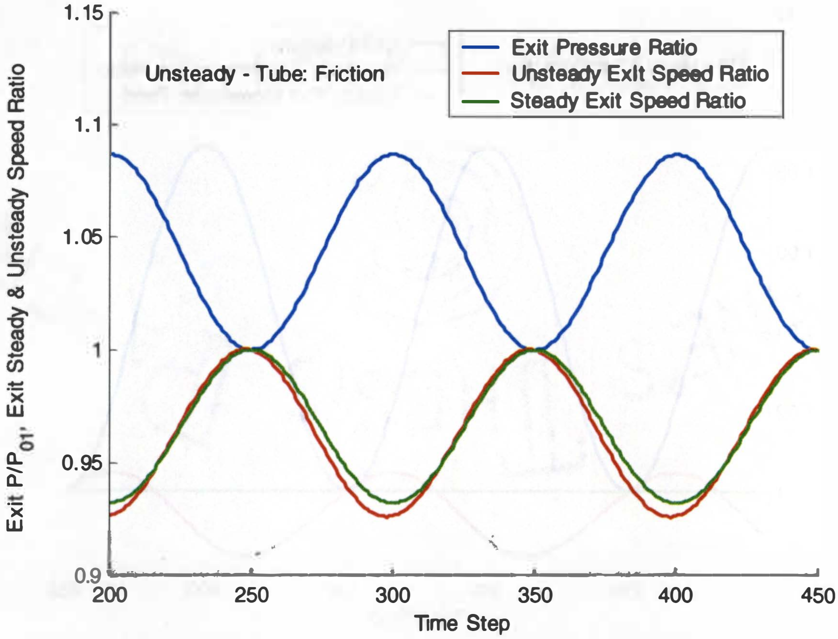

Figure 35. Unsteady constant area, adiabatic flow with friction – Back Pressure Ratio & Exit Speed Ratio.

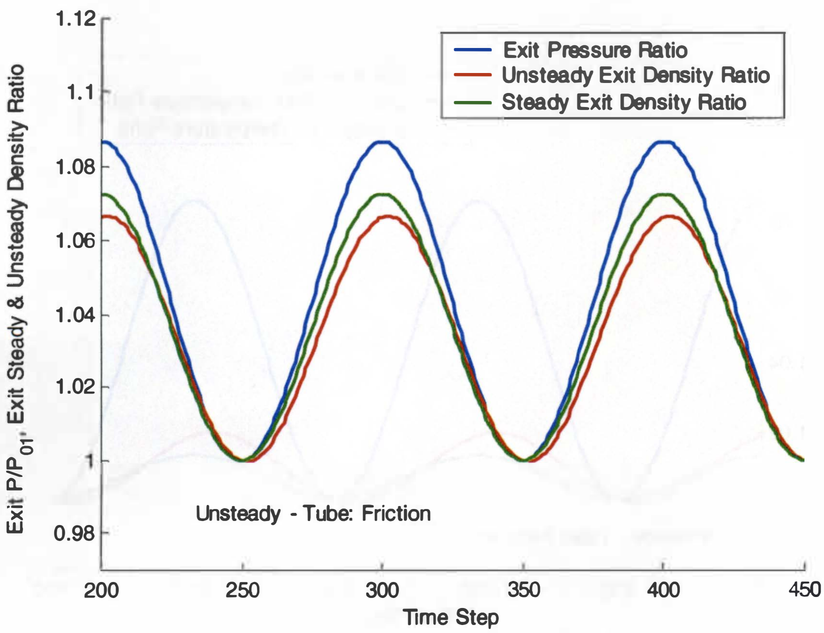

Figure 36. Unsteady constant area, adiabatic flow with friction – Back Pressure Ratio & Exit Density Ratio.

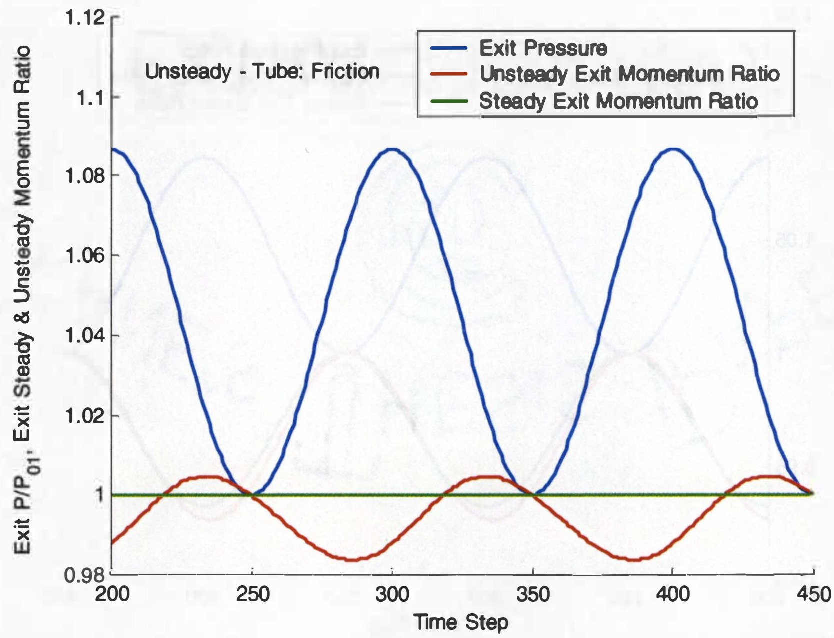

Figure 37. Unsteady constant area, adiabatic flow with friction – Back Pressure Ratio & Exit Momentum Ratio.

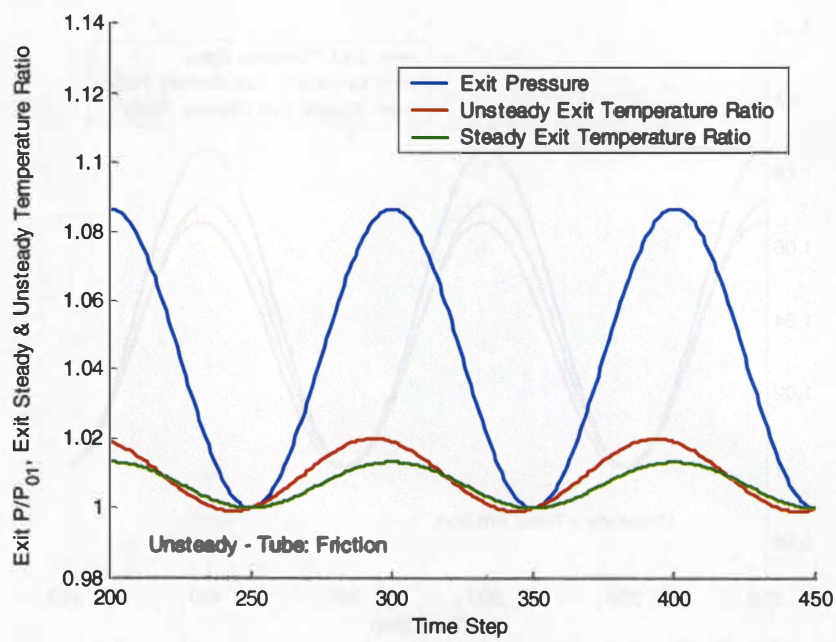

Figure 38. Unsteady constant area, adiabatic flow with friction – Back Pressure Ratio & Exit Temperature Ratio.

5.2.2 Unsteady adiabatic, frictionless flow in a convergent-divergent nozzle

Figure 39 shows the Mach number of the general flow in a convergent divergent nozzle. The Figure shows four flow stages for four different time steps and therefore four different back pressures. The same time steps will be used for all unsteady simulations in the convergent divergent nozzle

The four steps were selected to show an even transition in the flow. The black solid lines represent the steady flow property. Due to inertia effects, the unsteady flow shock is positioned behind the steady case. The normal shock is moving toward the outlet since the back pressure is decreasing from *0.88* to *0.65* as illustrated in Figure 39 and tabulated in Table 3. It appears that for curve (1), the unsteady flow is ahead of the steady; however, this is not the case because while the steady flow begins to move toward the outlet, the unsteady flow is still going toward the inlet. While Figure 38 shows the entire region of the flow, The pressure, density, and temperature graphs (Figures 39, 40, 41) show only the diverging part of the nozzle.

Table 3. Back pressure for the flow shown

Flow Position	Time Step	P_b / P_{01}
(1)	80	0.8800
(2)	88	0.8006
(3)	92	0.7295
(4)	100	0.6500

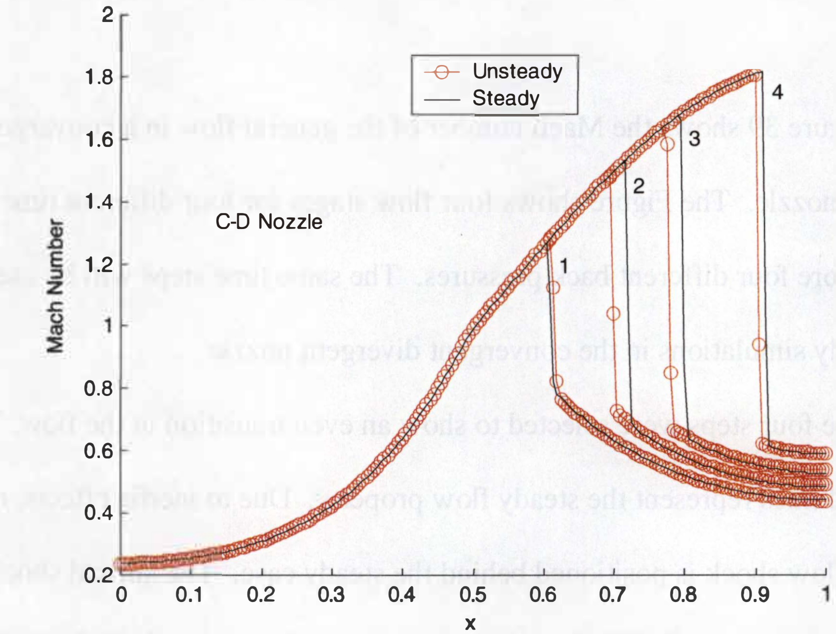

Figure 39. Unsteady adiabatic, frictionless flow in a C-D nozzle – Mach Number.

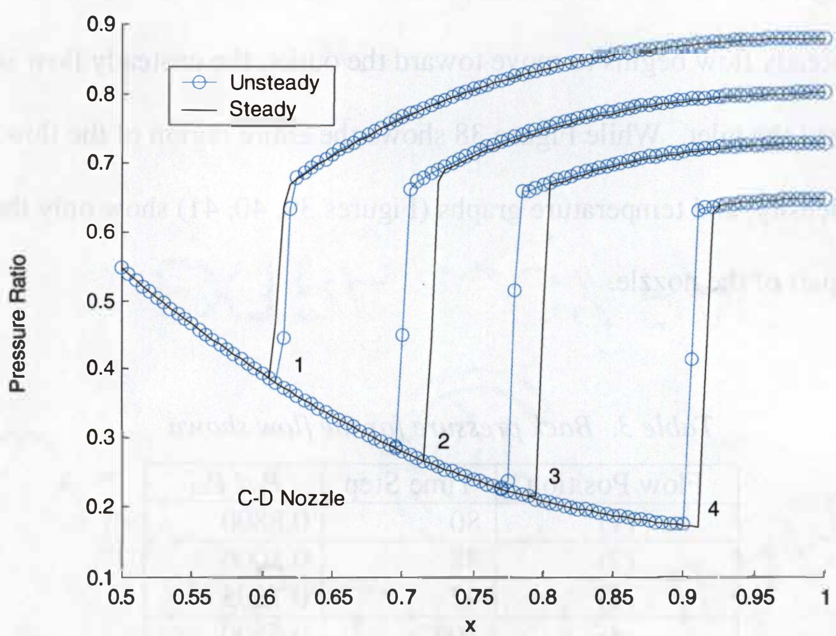

Figure 40. Unsteady adiabatic, frictionless flow in a C-D nozzle – Pressure Ratio.

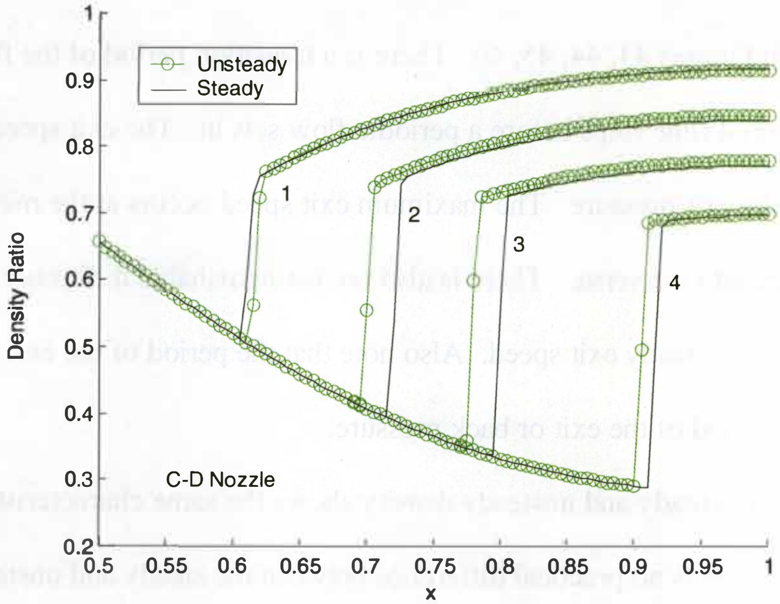

Figure 41. Unsteady adiabatic, frictionless flow in a C-D nozzle – Density Ratio.

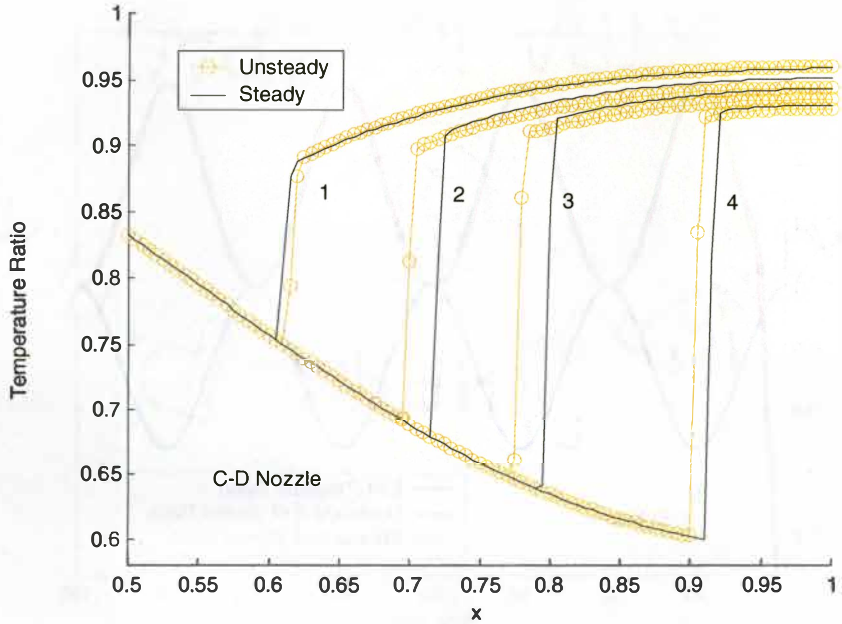

Figure 42. Unsteady adiabatic, frictionless flow in a C-D nozzle – Temperature Ratio.

The exit steady and unsteady speed, density, momentum, and temperature are plotted in Figures 43, 44, 45, 46. There is a transition period of the flow during the initial time steps before a periodic flow sets in. The exit speed acts the opposite as the exit pressure. The maximum exit speed occurs at the minimum exit pressure and vice versa. There is also no distinguishable difference between the steady and unsteady exit speed. Also note that the period of the exit speed is equal to the period of the exit or back pressure.

The exit steady and unsteady density shows the same characteristics of the exit speed. There is no practical difference between the steady and unsteady densities and they have the same period as the pressure; although the unsteady density is slightly out of phase.

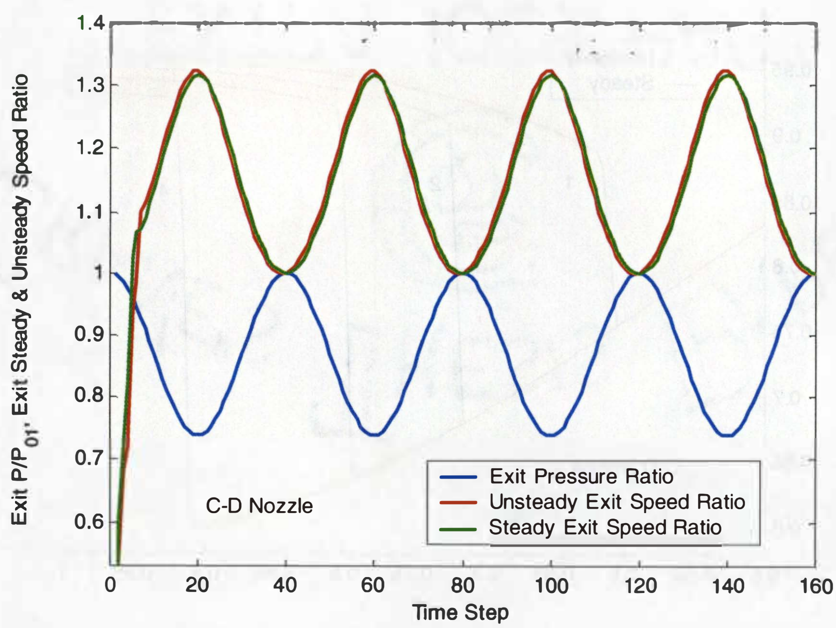

Figure 43. Unsteady adiabatic, frictionless flow in a C-D nozzle – Back Pressure Ratio & Exit Speed Ratio.

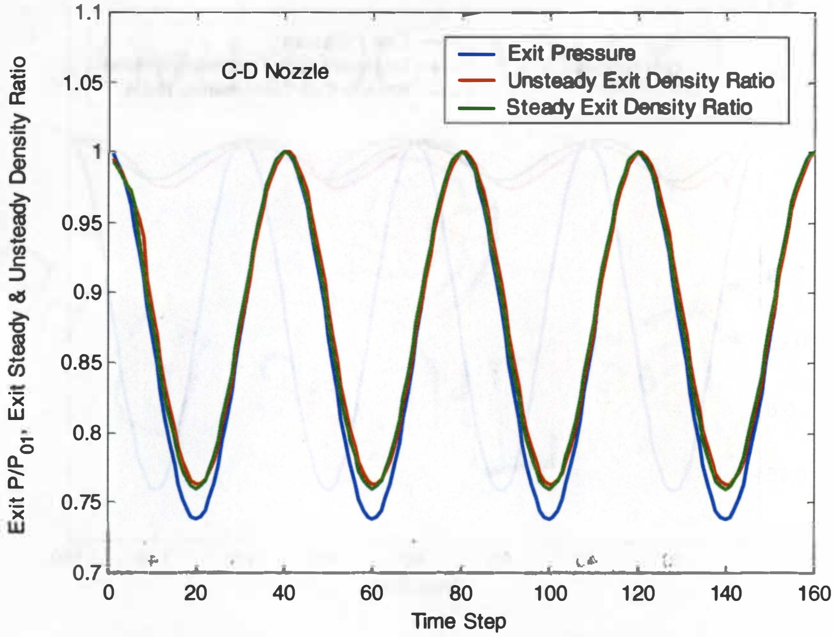

Figure 44. Unsteady adiabatic, frictionless flow in a C-D nozzle – Back Pressure Ratio & Exit Density Ratio.

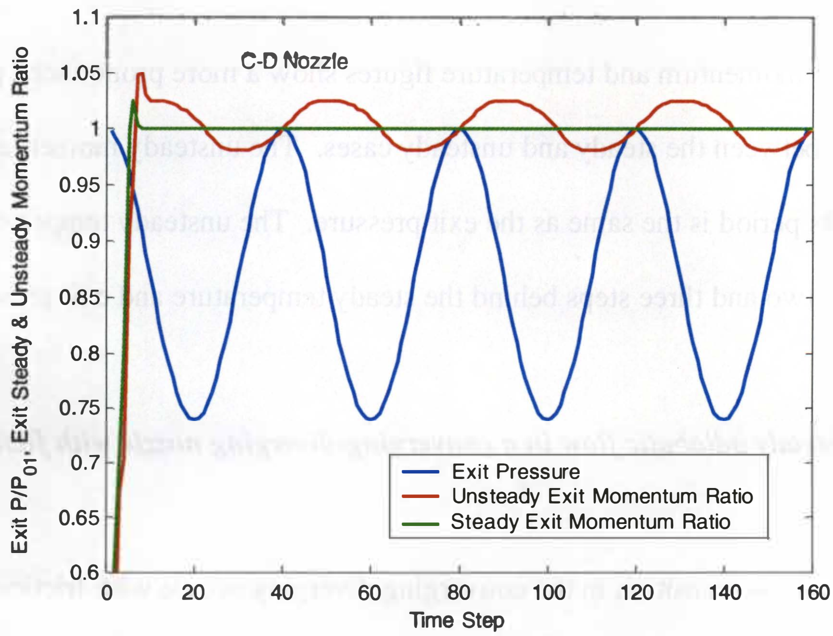

Figure 45. Unsteady adiabatic, frictionless flow in a C-D nozzle – Back Pressure Ratio & Exit Momentum Ratio.

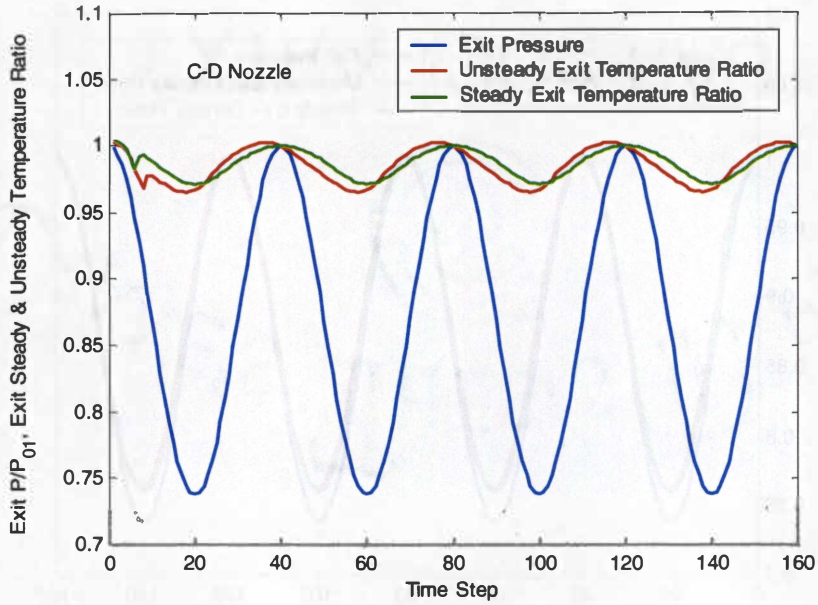

Figure 46. Unsteady adiabatic, frictionless flow in a C-D nozzle – Back Pressure Ratio & Exit Temperature Ratio.

The momentum and temperature figures show a more pronounced phase difference between the steady and unsteady cases. The unsteady momentum does vary and its period is the same as the exit pressure. The unsteady temperature lag is between two and three steps behind the steady temperature and exit pressure.

5.2.3 *Unsteady adiabatic flow in a converging-diverging nozzle with fiction*

The flow transition in the converging diverging nozzle with friction is depicted in Figure 47. As it was the case with the steady case in section 5.1.2, friction does not change the flow considerably for this nozzle. Density, momentum, and temperature are plotted in Figures 48, 49, 50. The Figures only show the diverging part of the nozzle. The same positioning effect by the unsteady flow is seen in this case. Refer to section 5.2.2 for the time and back pressure corresponding to the four curves detailed here.

Exit speed, density, momentum, and temperature are plotted in Figures 51, 52, 53, 54. As the case without friction, the unsteady exit speed and density are not significantly out of phase with the steady case, and have the same frequency as the back pressure. However, as expected, the unsteady momentum does change with pressure with the same frequency.

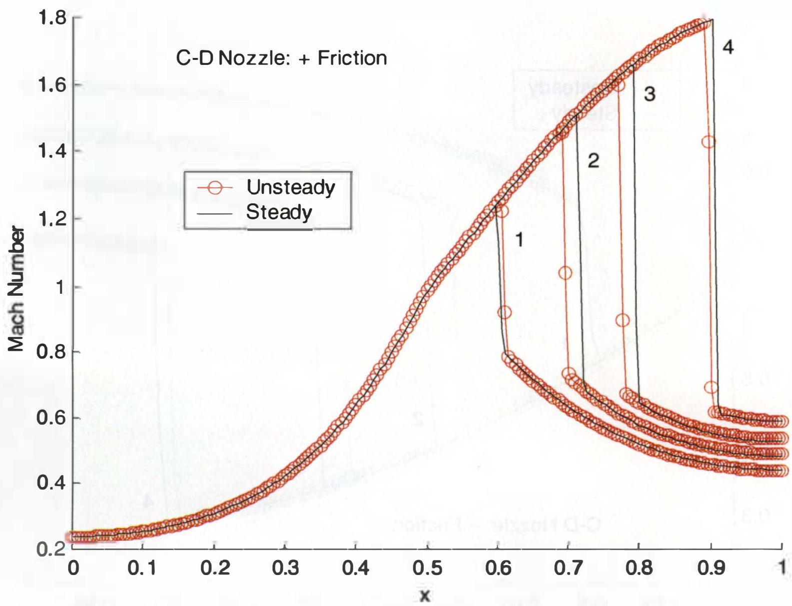

Figure 47. Unsteady adiabatic flow in a C-D nozzle with friction – Mach Number.

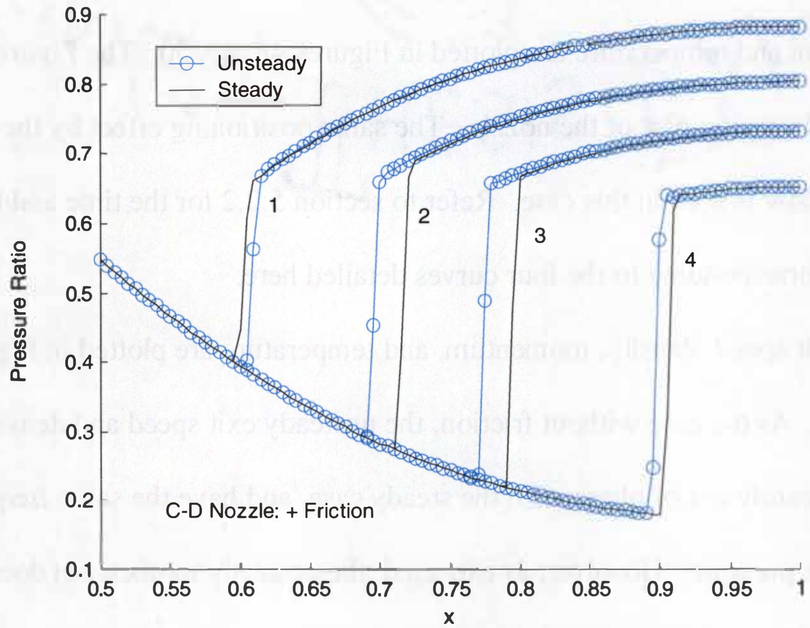

Figure 48. Unsteady adiabatic flow in a C-D nozzle with friction – Pressure Ratio.

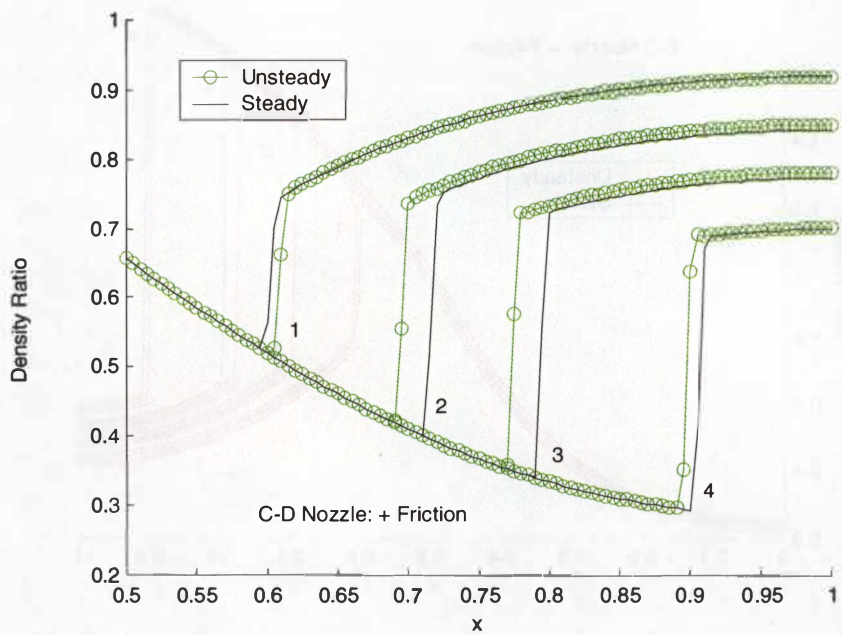

Figure 49. Unsteady adiabatic flow in a C-D nozzle with friction – Density Ratio.

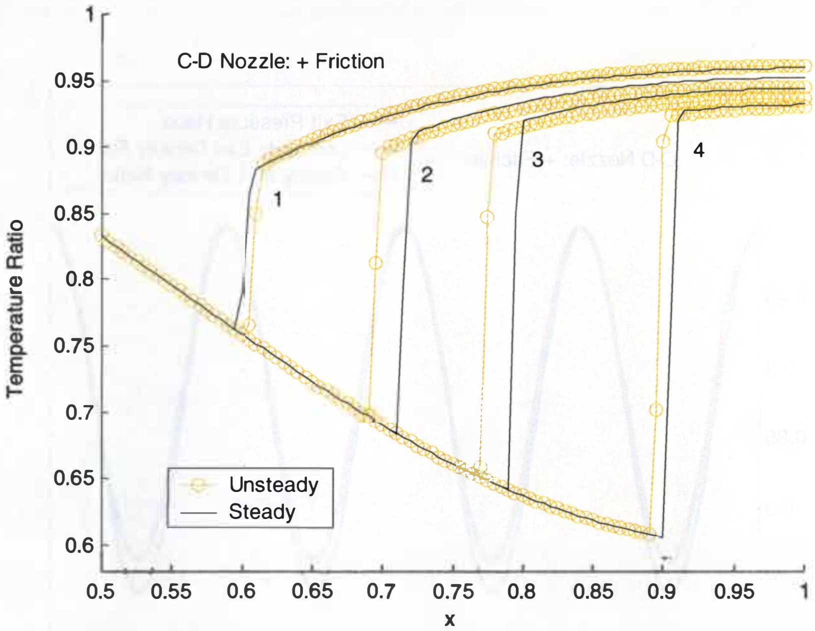

Figure 50. Unsteady adiabatic flow in a C-D nozzle with friction – Temperature Ratio.

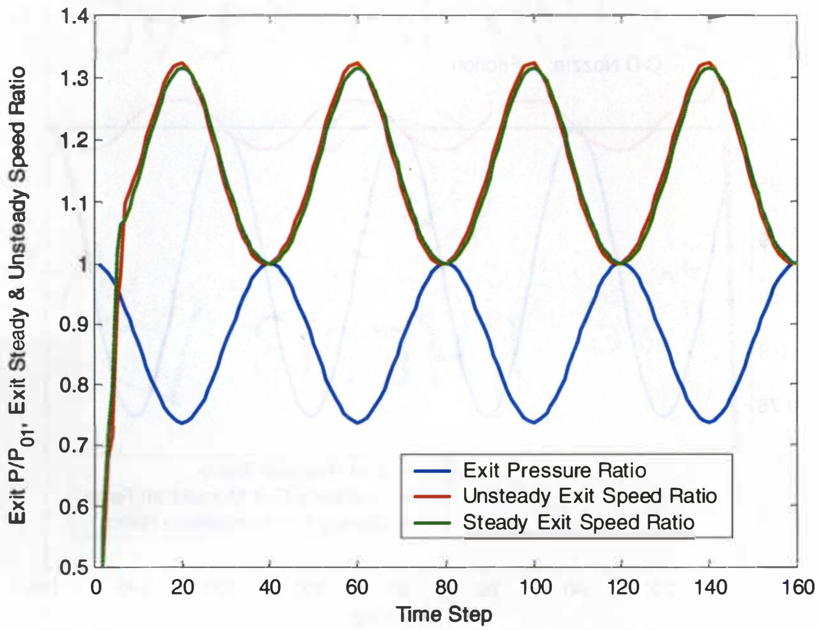

Figure 51. Unsteady adiabatic flow in a C-D nozzle with friction – Back Pressure Ratio & Exit Speed Ratio.

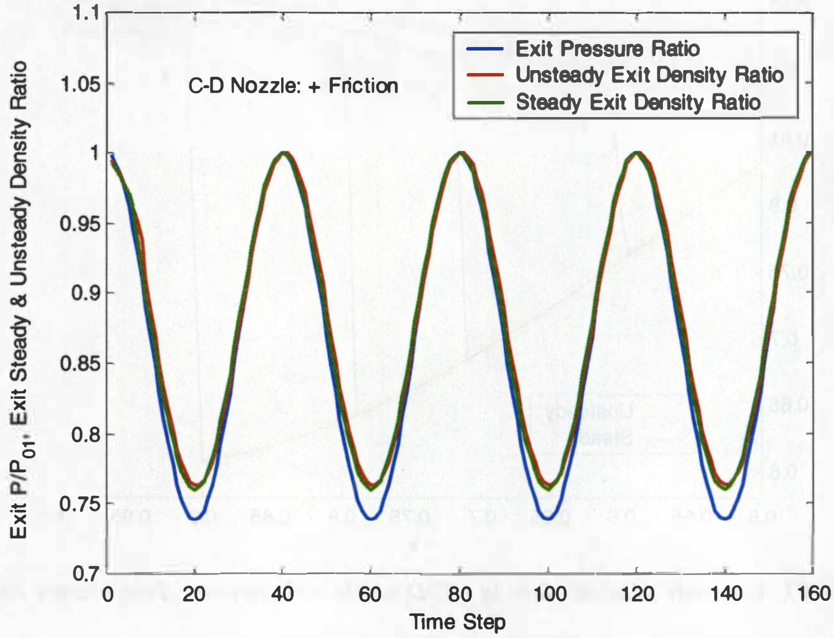

Figure 52. Unsteady adiabatic flow in a C-D nozzle with friction – Back Pressure Ratio & Exit Density Ratio.

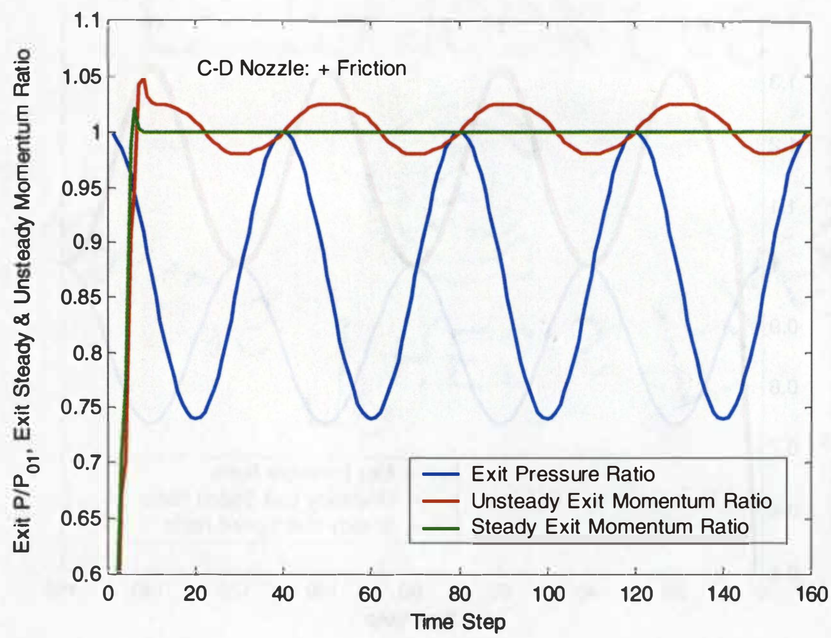

Figure 53. Unsteady adiabatic flow in a C-D nozzle with friction – Back Pressure Ratio & Exit Momentum Ratio.

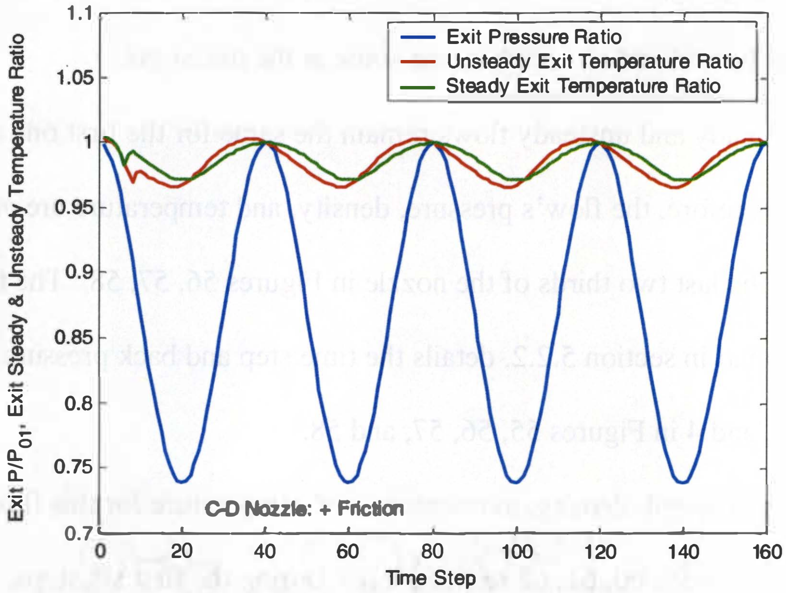

Figure 54. Unsteady adiabatic flow in a C-D nozzle with friction – Back Pressure Ratio & Exit Temperature Ratio.

5.2.4 Unsteady frictionless flow in a convergent-divergent nozzle with heat transfer

The flow is heated in the diverging part of the nozzle only. There is a change in the shockless flow at $x = 0.5$; this is due to the presence of the heat flux. Figure 55 shows the transition of the unsteady flow. The four positions of the flow were chosen at the same time station as the previous two simulations (Table 4). Flow at position (1) is at the highest back pressure $p = 0.88$ and the $p = 0.65$ for curve (4). For this range of back pressures, and in the absence of a heat flux, the flow remained choked at the throat. However, with the addition of heat flux, for the higher back pressures, the flow remains subsonic throughout the nozzle. This is seen in curve (1) and the unsteady (2). The steady curve (2) has already become choked and therefore a normal shock is present. The unsteady curve (2) is positioned behind and has not become sonic at the throat yet.

The steady and unsteady flows remain the same for the first one third of the nozzle, therefore, the flow's pressure, density, and temperature are only plotted over the last two thirds of the nozzle in Figures 56, 57, 58. The following table, also found in section 5.2.2, details the time step and back pressure of the curves 1,2,3, and 4 in Figures 55, 56, 57, and 58.

The exit speed, density, momentum, and temperature for this flow are plotted in Figures 59, 60, 61, 62 respectively. During the first six steps, the flow is transient before the periodic flow sets in. The steady and unsteady results for all properties have the same period as the back pressure. This behavior has been observed whether there is a heat flux or not. However, the unsteady exit speed is ~1.87% larger than the steady speed. The exit density is virtually the same between the steady and unsteady flow. The exit temperature exhibits a phase difference, the values for the steady and unsteady cases are the same.

Table 4. Back pressure for the flow shown

Flow Position	Time Step	P_b / P_{tot}
(1)	80	0.8800
(2)	88	0.8006
(3)	92	0.7295
(4)	100	0.6500

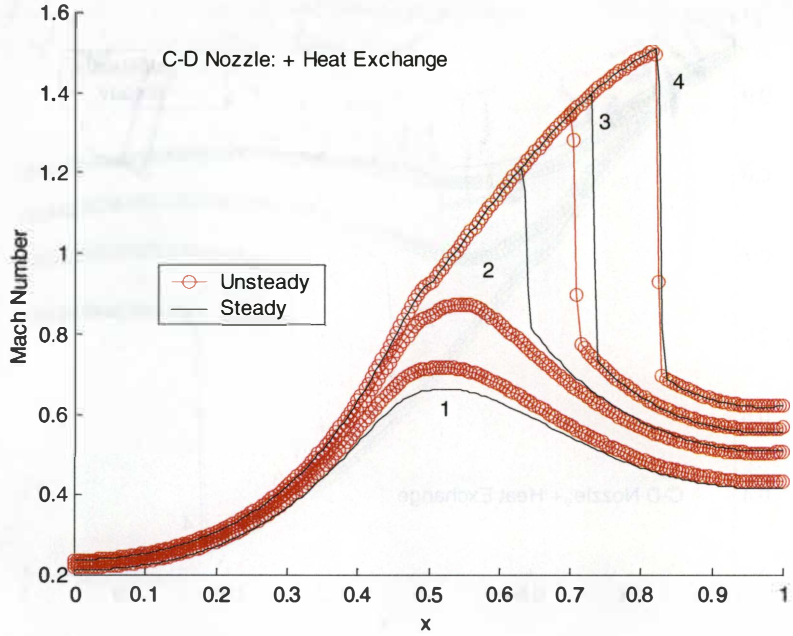

Figure 55. Unsteady frictionless flow in a C-D nozzle with heat transfer – Mach Number

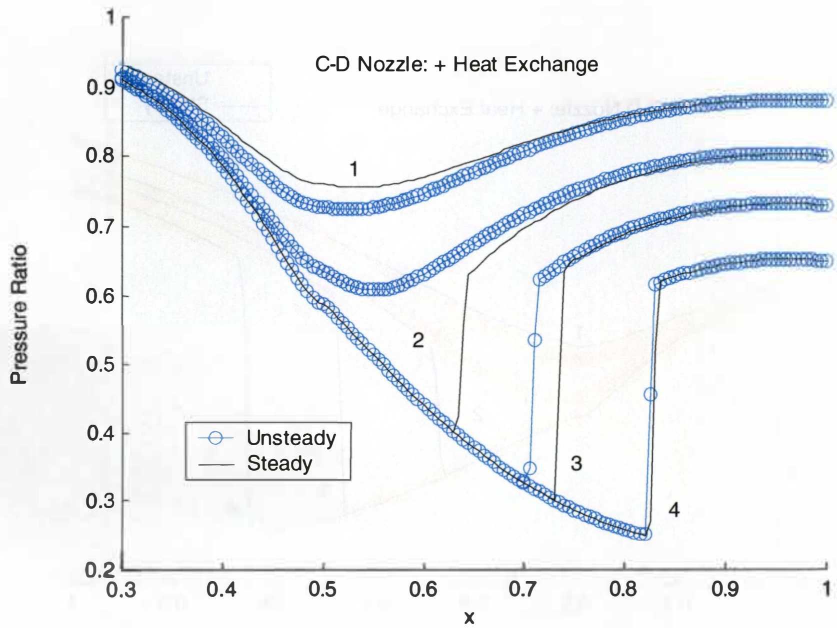

Figure 56. Unsteady frictionless flow in a C-D nozzle with heat transfer – Pressure Ratio.

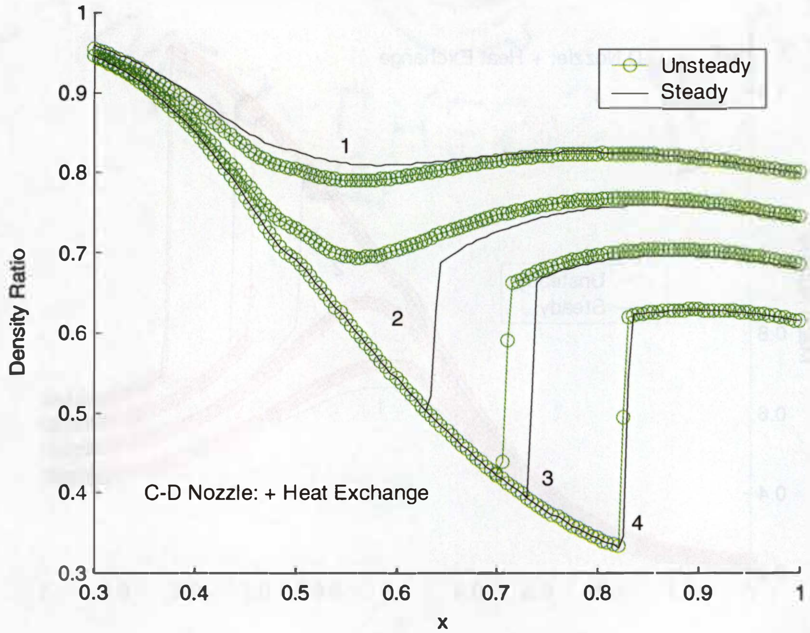

Figure 57. Unsteady frictionless flow in a C-D nozzle with heat transfer – Density Ratio.

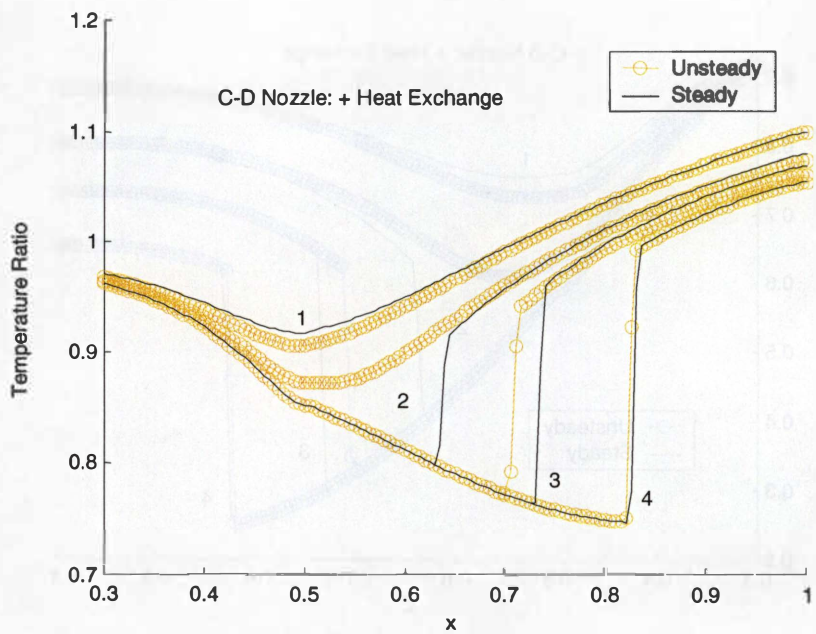

Figure 58. Unsteady frictionless flow in a C-D nozzle with heat transfer – Temperature Ratio.

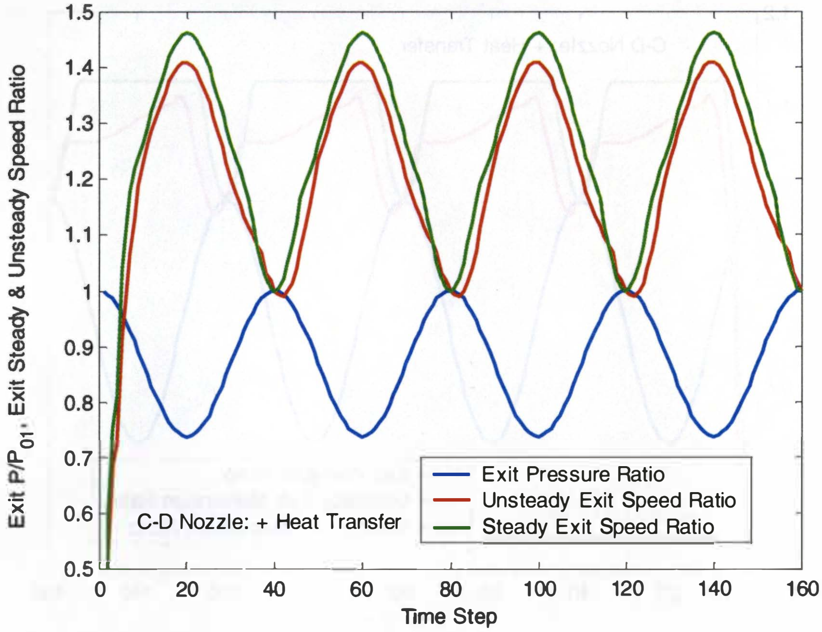

Figure 59. Unsteady frictionless flow in a C-D nozzle with heat transfer – Back Pressure Ratio & Exit Speed Ratio.

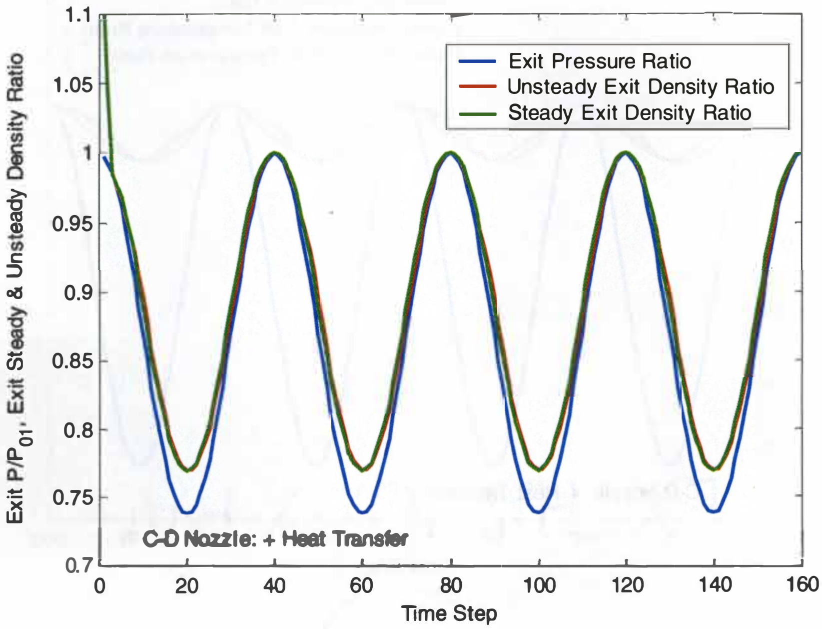

Figure 60. Unsteady frictionless flow in a C-D nozzle with heat transfer – Back Pressure Ratio & Exit Density Ratio.

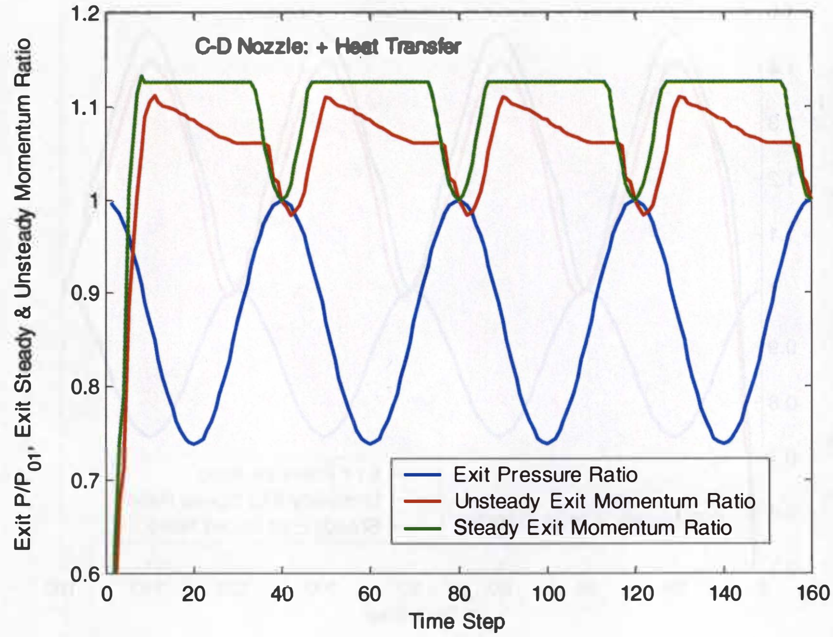

Figure 61. Unsteady frictionless flow in a C-D nozzle with heat transfer – Back Pressure Ratio & Exit Momentum Ratio.

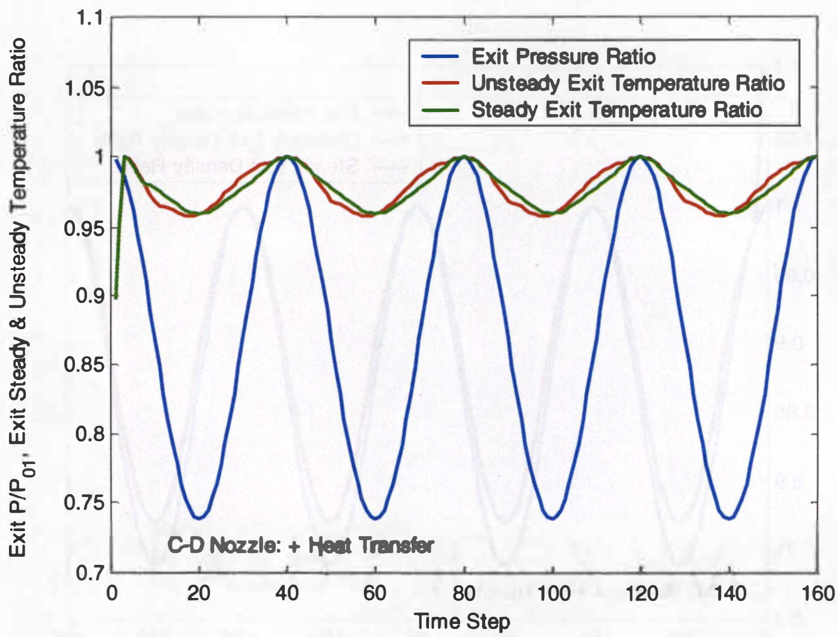

Figure 62. Unsteady frictionless flow in a C-D nozzle with heat transfer – Back Pressure Ratio & Exit Temperature Ratio.

Because the flow is no longer choked for a range of back pressures, the steady momentum is no longer constant for all time steps. While the flow is choked, the momentum is constant until the flow begins to turn subsonic. The momentum decreases as the flow goes from sonic to subsonic and increases as the flow goes from subsonic to sonic. This is expected since the maximum linear momentum is obtained when the flow is choked. The unsteady momentum is not constant at any point. The changes illustrated in Figure 61 are a combination of the flow being unsteady and the flow going from being choked to being subsonic.

5.2.5 Unsteady flow in a converging-diverging nozzle with friction and heat transfer.

The Mach number of the flow inside the nozzle with friction and heat transfer is illustrated in Figure 63. Because of the heat flux chosen, the flow is subsonic for high back pressures. The unsteady flow appeared to be ahead of the steady flow, but as in all previous cases, the steady Mach number is increasing while the unsteady flow Mach number is still decreasing. Again, this shift in the normal shock position is due to inertia. Figures 64, 65, and 66 illustrated the flow's density, pressure, and temperature along the nozzle.

The exit properties for the combined flow exhibit the same characteristics as the frictionless flow with heat transfer. As discussed earlier, the friction did not changed significantly. Exit speed, density, momentum, and temperature are plotted in Figures 67, 68, 69, and 70. The steady momentum did change for this flow, not because of the varying back pressure, but because the heat transfer did not allow the nozzle to be choked. The unsteady momentum displays this change in addition to the change due to the changing back pressure.

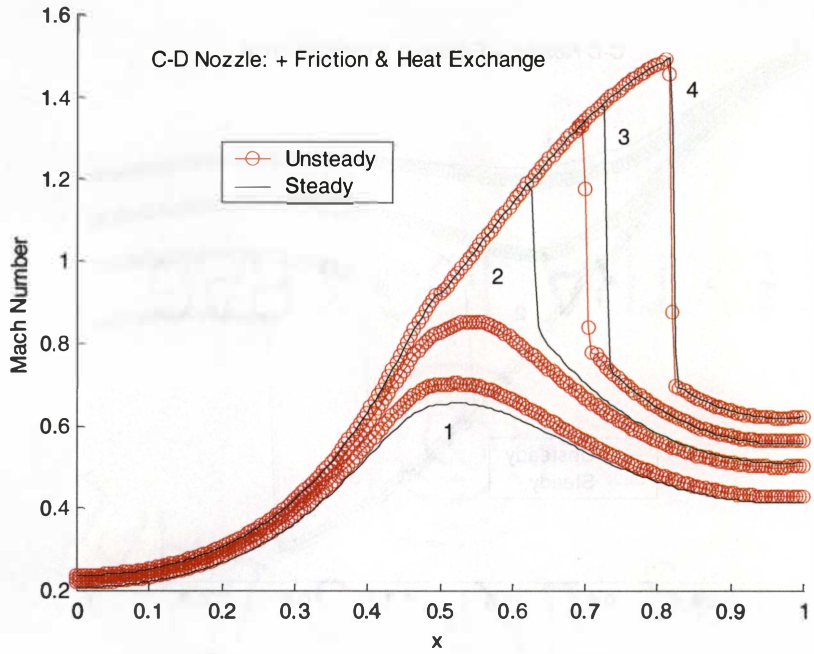

Figure 63. Unsteady flow in a C-D nozzle with friction and heat transfer – Mach Number.

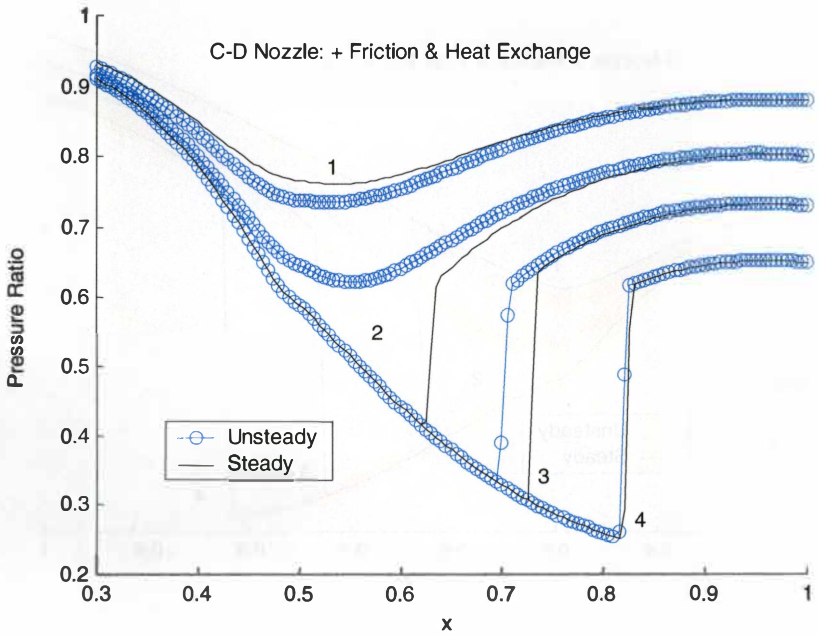

Figure 64. Unsteady flow in a C-D nozzle with friction and heat transfer – Pressure Ratio.

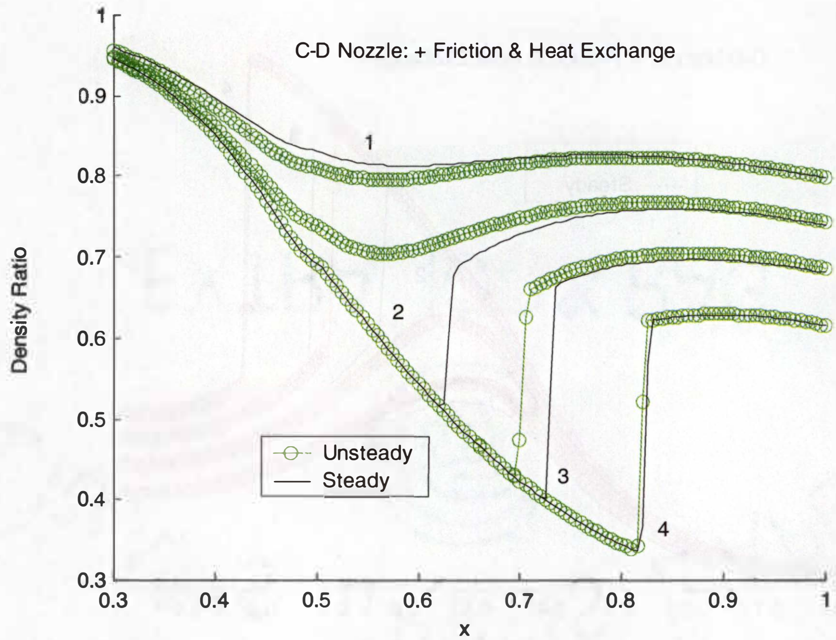

Figure 65. Unsteady flow in a C-D nozzle with friction and heat transfer – Density Ratio.

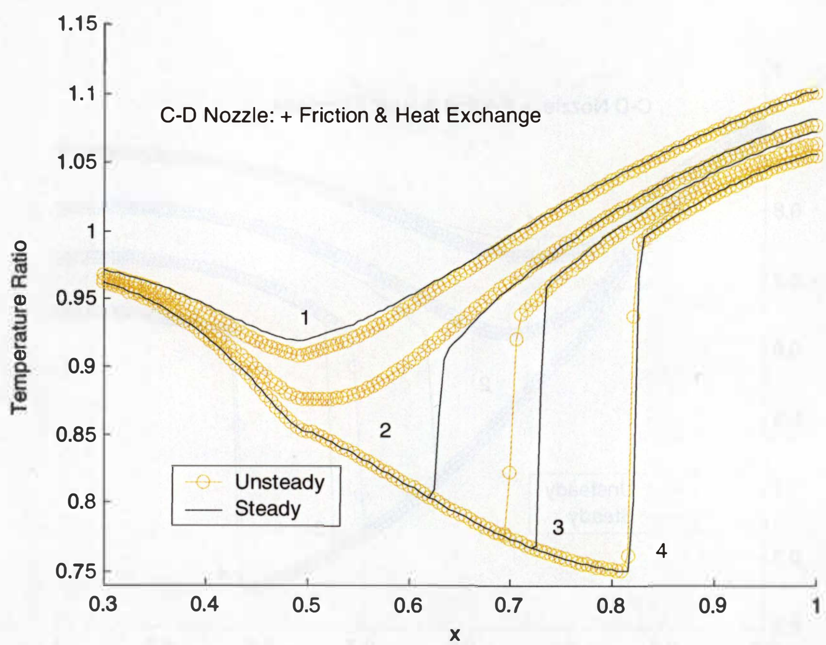

Figure 66. Unsteady flow in a C-D nozzle with friction and heat transfer – Temperature Ratio.

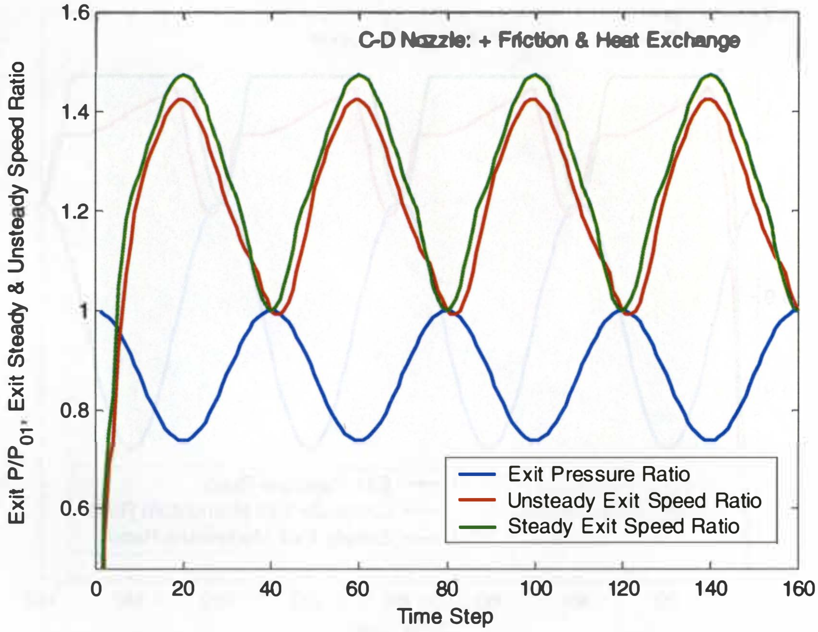

Figure 67. Unsteady flow in a C-D nozzle with friction and heat transfer – Back Pressure Ratio & Exit Speed Ratio.

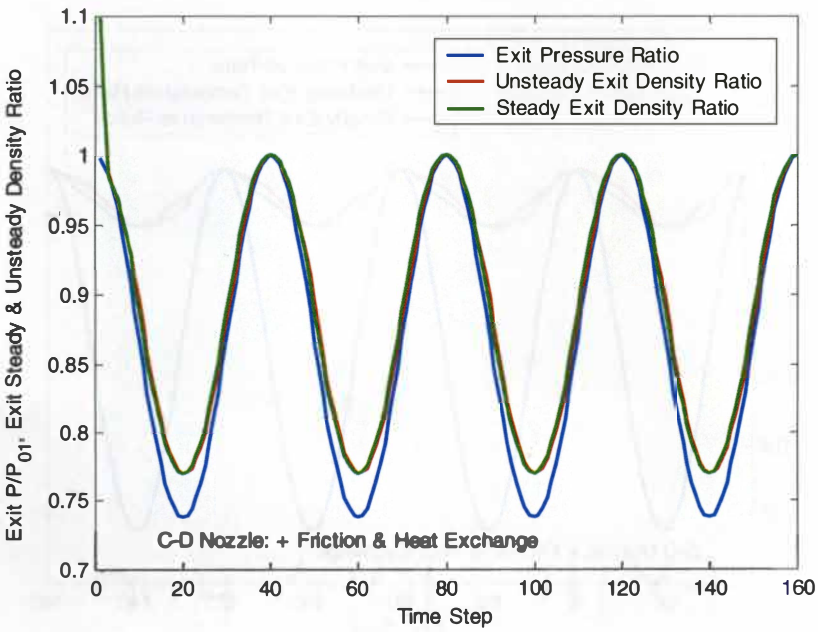

Figure 68. Unsteady flow in a C-D nozzle with friction and heat transfer – Bach Pressure Ratio & Exit Density Ratio.

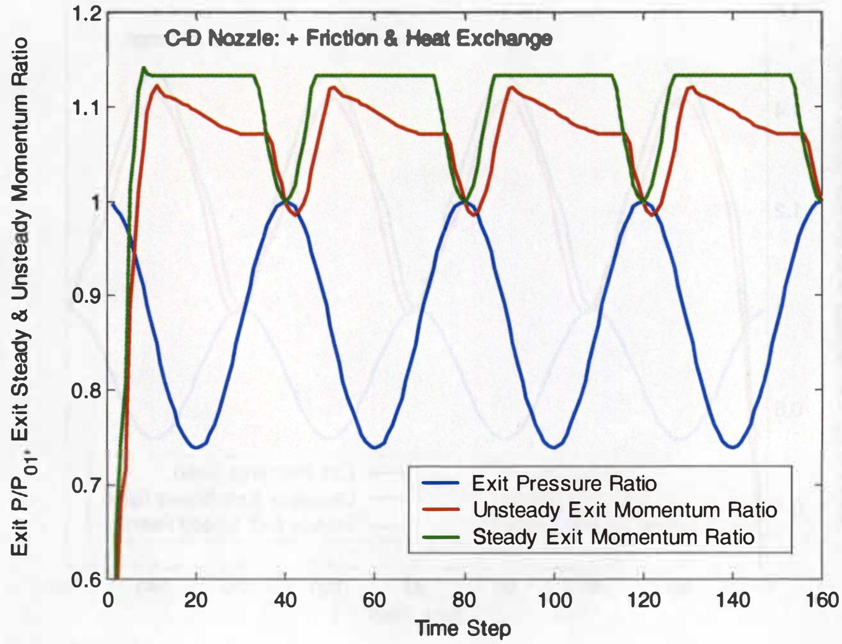

Figure 69. Unsteady flow in a C-D nozzle with friction and heat transfer –Back Pressure Ratio & Exit Momentum Ratio.

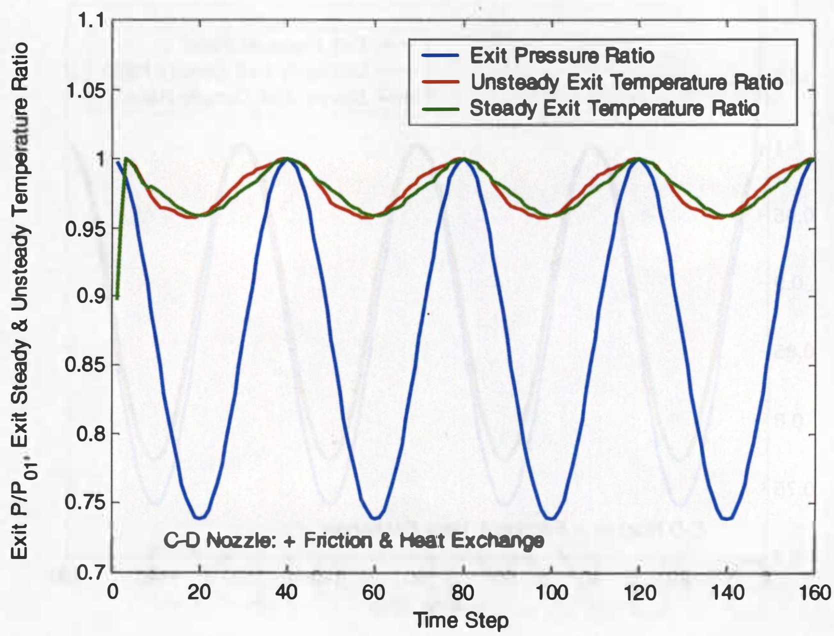

Figure 70. Unsteady flow in a C-D nozzle with friction and heat transfer – Back Pressure Ratio & Exit Temperature Ratio.

6. Conclusions

The generalized algorithm developed here allowed the investigation of complex quasi one-dimensional compressible flows with wall friction and heat transfer. This project modeled the combined effects of friction and heat transfer in a constant area tube and a convergent divergent nozzle.

6.1 Steady compressible flow conclusions

The effect of heat transfer was observed in a constant area tube with friction. Normal shocks move downstream with cooling and upstream with heating. The exit speed was found to be linearly dependent on the heat flux applied.

For a convergent-divergent nozzle with an exit area to throat area ratio of 1.5, friction does not have a significant impact on the flow. A change of 5,000% change in friction had a less than 1.0 % change in exit speed and density. Perhaps for area ratios close to 1.0, friction would be more significant. However, for this convergent-divergent nozzle, a 100% increase in heat flux decreased the exit density by ~10% and increased exit speed by ~10%. While friction effects depend on the geometry of the nozzle and roughness of the wall, heat transfer is only a function of the magnitude of the heat flux. Therefore, heat transfer does have an impact in any type of conventional nozzle whereas friction may or may not have a significant effect in a quasi one-dimensional compressible flow.

6.2 Unsteady compressible flow conclusions.

Five unsteady compressible flows with a periodic sinusoidal back pressure were investigated. An important question was how exit speed, density, momentum, and temperature varied. It was observed in all five cases that the unsteady flow normal shock was positioned behind its steady counterpart inside the duct. This phase difference is due to inertia and was observed for Mach number, pressure, density, and temperature.

The exit pressure was equal by design for the steady and unsteady flows. The difference in position between steady and unsteady exit speed and density was minimal while the unsteady exit temperature was clearly out of phase with the steady temperature. The steady momentum remained constant for choked flow, but the unsteady momentum followed the frequency of the back pressure. Whether the flow was affected by varying cross-sectional area, friction, or heat transfer; exit speed, density, momentum, and temperature had the same fundamental frequency as the periodic sinusoidal back pressure.

6.3 Recommendations for further study.

The converging-diverging nozzle used in this investigation had an outlet to throat ratio of 1.5. Friction effects did not change the flow substantially. An important step should be to investigate friction effects with nozzles of smaller ratios to determine the range where friction should be considered an important design parameter.

All unsteady flows were shocked. While shocked flows are more difficult to investigate, the back pressure equals the exit pressure because the flow is subsonic at the outlet. The unsteady effects on a flow with a supersonic exit Mach number should also be analyzed.

The compressible flows were modeled as quasi one dimensional. The next step in this investigation should be to adapt the generalized algorithm for two and three dimensional analysis.

Bibliography

[1] Iannelli, Joe, 'A CFD Euler Solver from a Physical Acoustics-Convection Flux Jacobian Decomposition', International Journal for Numerical Methods in Fluids, *int. J. Numer. Meth. Fluids* ***31*****:** 821-860, 1999

[2] Oosthuizen, Patrick H. and Carscallen, William E., 'Compressible Fluid Flow', McGraw-Hill Companies Inc., New York, 1997.

[3] Hill, Philip G. and Peterson, Carl R., 'Mechanics and Thermodynamics of Propulsion', Addison-Wesley Publishing, Reading, 1992.

[4] John, James E.A.,'Gas Dynamics',Prentice-Hall, Englewood Cliffs, 1984.

[5] Zucrow, Maurice J. and Hoffman, Joe D., 'Gas Dynamics, vol. I', John Wiley & Sons, New York,1976.

[6] Shapiro, Ascher H., 'The Dynamics and Thermodynamics of Compressible Fluid Flow', The Ronald Press Company, New York, 1953.

Vita

Nefi Negrete was born in Leon Guanajuato, Mexico on November 23, 1976. He went to grade school and junior high school at Instituto America in Leon. He immigrated to the United States in November 1990. He graduated from Rhea County High School in 1995. From there, he went to the University of Tennessee, Knoxville and received a B.S. in aerospace engineering with a minor in business in 1999 and a M.S. in mechanical engineering in 2002.

5176 3768 16
09/24/02 MAB